

## RESEARCH ARTICLE

## Cellular and Molecular Properties of Neurons

Cholinergic depolarization recruits a persistent  $\text{Ca}^{2+}$  current in *Aplysia* bag cell neuronsKelly H. Lee, David E. Wassef, Eammon K. MacNeil, and  Neil S. Magoski

Department of Biomedical and Molecular Sciences, Experimental Medicine Graduate Program, Queen's University, Kingston, Ontario, Canada

## Abstract

Many behaviors and types of information storage are mediated by lengthy changes in neuronal activity. In bag cell neurons of the hermaphroditic sea snail *Aplysia californica*, a transient cholinergic synaptic input triggers an ~30-min afterdischarge. This causes these neuroendocrine cells to release egg laying hormone and elicit reproductive behavior. When acetylcholine is pressure-ejected onto a current-clamped bag cell neuron, the evoked depolarization is far longer than the current evoked by acetylcholine under voltage clamp, suggesting recruitment of another conductance. Our earlier studies found bag cell neurons to display a voltage-dependent persistent  $\text{Ca}^{2+}$  current. Hence, we hypothesized that this current is activated by the acetylcholine-induced depolarization and sought a selective  $\text{Ca}^{2+}$  current blocker. Rapid  $\text{Ca}^{2+}$  current evoked by 200-ms depolarizing steps in voltage-clamped cultured bag cell neurons demonstrated a concentration-dependent sensitivity to  $\text{Ni}^{2+}$ ,  $\text{Co}^{2+}$ ,  $\text{Zn}^{2+}$ , and verapamil but not  $\text{Cd}^{2+}$  or  $\omega$ -conotoxin G1Va. Leak subtraction of  $\text{Ca}^{2+}$  current evoked by 10-s depolarizing steps using the  $\text{IC}_{100}$  (concentration required to eliminate maximal current) of  $\text{Ni}^{2+}$ ,  $\text{Co}^{2+}$ ,  $\text{Zn}^{2+}$ , or verapamil revealed persistent  $\text{Ca}^{2+}$  current, demonstrating persistent current block. Only  $\text{Co}^{2+}$  and  $\text{Zn}^{2+}$  did not suppress the acetylcholine-induced current, although  $\text{Zn}^{2+}$  appeared to impact additional channels. When  $\text{Co}^{2+}$  was applied during an acetylcholine-induced depolarization, the amplitude was reduced; furthermore, protein kinase C activation, previously established to enhance the persistent  $\text{Ca}^{2+}$  current, extended the depolarization. Therefore, the persistent  $\text{Ca}^{2+}$  current sustains the acetylcholine-induced depolarization and may translate brief cholinergic input into afterdischarge initiation. This could be a general mechanism of triggering long-term change in activity with a short-lived input.

**NEW & NOTEWORTHY** Ionotropic acetylcholine receptors mediate brief synaptic communication, including in bag cell neurons of the sea snail *Aplysia*. However, this study demonstrates that cholinergic depolarization can open a voltage-gated persistent  $\text{Ca}^{2+}$  current, which extends the bag cell neuron response to acetylcholine. Bursting in these neuroendocrine cells results in hormone release and egg laying. Thus, this emphasizes the role of ionotropic signaling in reaching a depolarized level to engage  $\text{Ca}^{2+}$  influx and perpetuating the activity necessary for behavior.

acetylcholine receptor; mollusk; peptidergic neuron; prolonged depolarization; reproduction

## INTRODUCTION

Long-term change of neural activity in response to a brief stimulation underlies many nervous system functions and behaviors. In these instances, an input essentially triggers some form of tonic conductance, which results in plateau potentials, prolonged spiking, or afterdischarges. For example, cholinergic metabotropic/muscarinic receptors activate persistent  $\text{Ca}^{2+}$  current and/or nonselective cationic currents to support bursting in rat layer V pyramidal neurons

from medial prefrontal cortex (1), prolonged spiking of rat entorhinal cortex implicated in working memory (2, 3), elevation of firing in mouse corticopontine neurons that may participate in executive attention (4), and extension of activity in mouse primary auditory cortex neurons potentially involved in sensory learning (5). However, except for a few studies, such as those in hippocampal stratum oriens/alveus interneurons (6) or ventral tegmental dopaminergic neurons (7), it is relatively rare to observe an ionotropic/nicotinic cholinergic receptor causing similar responses. Here, we use bag

cell neurons from the sea snail *Aplysia californica* to show that an ionotropic acetylcholine receptor can mediate the transition from initial depolarization to lengthy response much like its metabotropic counterpart.

Bag cell neurons are neuroendocrine cells that are normally silent, with a resting potential of approximately  $-60$  mV, but after a cholinergic input from the pleuroabdominal connectives they undergo a collective 20- to 30-mV depolarization and  $\sim 30$ -min afterdischarge (8–10). Intracellular  $\text{Ca}^{2+}$  levels peak during the first few minutes of the afterdischarge and initiate the downstream effects that sustain much of the response (11). A train of action potentials analogous to the start of an afterdischarge causes voltage-gated  $\text{Ca}^{2+}$  influx, which gates voltage-independent, nonselective cationic current to drive a prolonged depolarization (12). High  $\text{Ca}^{2+}$  is maintained by  $\text{Ca}^{2+}$ -dependent mobilization from the endoplasmic reticulum and mitochondria (13, 14), as well as recruitment of covert  $\text{Ca}^{2+}$  channels to the plasma membrane by protein kinase C (PKC) (15–17). This leads to the activation of both voltage-independent (18, 19) and voltage-dependent nonselective cation channels (20–22). Ultimately, the accumulation of intracellular  $\text{Ca}^{2+}$  ensures the release of egg laying hormone and reproductive behavior (17, 23–25).

Although solely responsible for triggering afterdischarges in bag cell neurons, the acetylcholine receptor does not inherently produce the initial peak in  $\text{Ca}^{2+}$  levels that engage various cation channels. In particular, the acetylcholine-induced current is due to an ionotropic receptor, lasts  $\sim 1.5$  min, and is selective for monovalent cations (10, 26). Hence, both the short duration and  $\text{Ca}^{2+}$  impermeability preclude this receptor from contributing directly to  $\text{Ca}^{2+}$  influx, suggesting that it is necessary for separate  $\text{Ca}^{2+}$  conductance(s) to couple the cholinergic signal to intracellular pathways.

In our prior work, we found that bag cell neurons exhibit a persistent  $\text{Ca}^{2+}$  current, which can be opened by modest depolarization under voltage clamp (27). The present study demonstrates that the acetylcholine-induced depolarization recruits this persistent  $\text{Ca}^{2+}$  conductance under current clamp. We show that the duration of depolarization is shortened by  $\text{Co}^{2+}$ , a  $\text{Ca}^{2+}$  channel blocker that effectively antagonizes the persistent  $\text{Ca}^{2+}$  current but has no impact on the acetylcholine-induced current. Conversely, the duration of depolarization and number of action potentials are increased by a PKC activator, which was previously found to enhance the persistent  $\text{Ca}^{2+}$  current (27). Therefore, an ionotropic acetylcholine receptor can engage a voltage-dependent process to generate an extended period of activity.

## METHODS

### Animals and Cell Culture

Adult *A. californica* weighing 150–500 g were obtained from Marinus (Long Beach, CA) and housed in an  $\sim 300$ -L aquarium containing continuously circulating, aerated seawater (Instant Ocean; Aquarium Systems Inc, Mentor, OH) at  $18^\circ\text{C}$  on a 12:12-h light-dark cycle and fed romaine lettuce daily. All experiments were approved by the Queen's University Animal Care Committee (protocols 2017-1745 and 2021-2140).

For primary cultures of isolated bag cell neurons, animals were anesthetized by an injection of isotonic  $\text{MgCl}_2$  ( $\sim 50\%$

body wt; 390 mM), and the abdominal ganglion was removed and incubated for 18 h at  $22^\circ\text{C}$  in neutral protease (13.33 mg/mL; 4942078001, Roche/Sigma-Aldrich; St. Louis, MO or Oakville, ON, Canada) dissolved in tissue culture artificial seawater (tcASW) [composition in mM: 460 NaCl, 10.4 KCl, 11  $\text{CaCl}_2$ , 55  $\text{MgCl}_2$ , and 15 *N*-2-hydroxyethylpiperazine-*N'*-2-ethanesulfonic acid (HEPES), with 1 mg/mL glucose, 100 U/mL penicillin, and 0.1 mg/mL streptomycin; pH 7.8 with NaOH]. The ganglion was then transferred to fresh tcASW, and the bag cell neuron clusters were microdissected from the surrounding connective tissue. With a fire-polished Pasteur pipette and gentle trituration, neurons were dispersed onto  $35 \times 10$ -mm polystyrene tissue culture dishes (430165, Falcon-Corning; Fisher Scientific, Ottawa, ON, Canada) filled with tcASW. Neurons were maintained in tcASW for 1–3 days in a  $14^\circ\text{C}$  incubator, and experiments were performed on  $\geq 1$  day in vitro. Salts were obtained from Acros Organics (Morris Plains, NJ), Fisher Scientific, or Sigma-Aldrich.

### Whole Cell Voltage-Clamp Recordings

Voltage-clamp recordings were made with an EPC-8 amplifier (HEKA Elektronik/Harvard Apparatus; St. Laurent, QC, Canada) and the tight-seal, whole cell method. Microelectrodes were pulled from 1.12-mm-internal diameter and 1.5-mm-external diameter borosilicate glass capillaries (TW150F-4; World Precision Instruments; Sarasota, FL) and had a resistance of 1–2 M $\Omega$  when filled with various intracellular salines (see below). Pipette junction potentials were nulled and, subsequent to seal formation, pipette capacitive currents were canceled. After breakthrough neuronal capacitance was also canceled, and the series resistance (3–5 M $\Omega$ ) was compensated to 80% and monitored throughout the experiment. Current was filtered at 1 kHz with the EPC-8 built-in Bessel filter and sampled at 1 or 2 kHz with a Digidata 1440 analog-to-digital converter (Molecular Devices, Sunnyvale, CA), a Windows-based personal computer, and Clampex software (v10.7; Molecular Devices). Clampex was also used to control the membrane potential under voltage clamp (see RESULTS for details).

$\text{Ca}^{2+}$  currents were isolated with an extracellular saline of  $\text{Ca}^{2+}$ - $\text{Cs}^+$ -tetraethylammonium (TEA) artificial seawater (ASW), where the  $\text{Na}^+$  was replaced with TEA and the  $\text{K}^+$  with  $\text{Cs}^+$  (composition in mM: 460 TEA-Cl, 10.4 CsCl, 55  $\text{MgCl}_2$ , 11  $\text{CaCl}_2$ , 15 HEPES, pH 7.8 with CsOH). The pipette solution was a  $\text{Cs}^+$ -aspartate (Asp)-based intracellular saline [composition in mM: 70 CsCl, 10 HEPES, 11 glucose, 10 glutathione, 5 ethylene glycol-bis( $\beta$ -aminoethylether)-*N,N,N'*-tetraacetic acid (EGTA), 500 aspartic acid, 5 adenosine 5'-triphosphate  $2\text{Na}\cdot\text{H}_2\text{O}$  (ATP) (grade 2; A3377, Sigma-Aldrich), and 0.1 guanosine 5'-triphosphate  $\text{Na}\cdot\text{H}_2\text{O}$  (GTP) (type 3; G8877, Sigma-Aldrich), pH 7.3 with CsOH]. The free  $\text{Ca}^{2+}$  concentration was set at 300 nM by adding 3.32 mM  $\text{CaCl}_2$ , as calculated with WebMaxC (<https://somapp.ucdmc.ucdavis.edu/pharmacology/bers/maxchelator/webmaxc/webmaxcS.htm>). Upon breakthrough, neurons were dialyzed for 10 min before recording. A junction potential of 20 mV between  $\text{Ca}^{2+}$ - $\text{Cs}^+$ -TEA ASW and  $\text{Cs}^+$ -Asp was compensated for by subtraction offline. However, for rapid, voltage-gated  $\text{Ca}^{2+}$  currents, subtraction of leak current was performed online with a *P/4* protocol from a holding potential of  $-60$  mV, with subpulses of opposite polarity and one-fourth the magnitude, as well as an

intersubpulse interval of 500 ms and 100 ms before actual test pulses. Persistent  $\text{Ca}^{2+}$  currents were measured by delivering 10-s voltage steps before and after block by a saturating concentration of  $\text{Co}^{2+}$ ,  $\text{Ni}^{2+}$ , verapamil, or  $\text{Zn}^{2+}$  and then subtracting the blocked current from control to eliminate leak current (see RESULTS for details).  $\text{Ca}^{2+}$  influx during cholinergic-like depolarization was achieved by delivering a series of voltage ramps that mimicked the acetylcholine-evoked membrane potential changes under sharp-electrode recordings from White and Magoski (10) and White et al. (28) (see RESULTS for details).

Acetylcholine-induced currents were measured with normal ASW (nASW; composition as per tcASW but with the glucose, penicillin, and streptomycin omitted) in the bath and a  $\text{K}^+$ -Asp-based intracellular solution (composition in mM: 500  $\text{K}^+$ -Asp, 70 KCl, 1.25  $\text{MgCl}_2$ , 10 HEPES, 11 glucose, 10 glutathione, 5 EGTA, 5-ATP, and 0.1 GTP, with 300 nM free  $\text{Ca}^{2+}$ ; pH 7.3 with KOH) in the pipette. Upon breakthrough, the neurons were again dialyzed for 10 min before recording. A junction potential of 15 mV was again compensated for by subtraction offline. No leak subtraction was performed while recording these currents.

### Sharp-Electrode Current-Clamp Recordings

Current-clamp recordings were made in nASW with an Axoclamp 2B (Molecular Devices) amplifier and the sharp-electrode bridge-balanced method. Microelectrodes were pulled from 0.9-mm-internal diameter and 1.2-mm-external diameter borosilicate glass capillaries (TW120F-4, World Precision Instruments) and had a resistance of 5–20 M $\Omega$  when filled with 2 M  $\text{K}^+$ -acetate plus 10 mM HEPES and 100 mM KCl (pH 7.3 with KOH). Hyperpolarizing current pulses for bridge balance were delivered with a S88 stimulator (Grass, Quincy, MA); in addition, neurons were initially set to  $-60$  mV with constant bias current from the Axoclamp DC current command, if necessary. Voltage was filtered at 3 kHz with the Axoclamp built-in Bessel filter and sampled at 2 kHz as described in *Whole Cell Voltage-Clamp Recordings* for membrane current.

### $\text{Ca}^{2+}$ Imaging

For  $\text{Ca}^{2+}$  imaging, fura-PE3- $\text{K}^+$  salt was dissolved at 1 mM in the  $\text{K}^+$ -Asp-based intracellular solution and introduced by a 30-min dialysis via the whole cell pipette under voltage clamp at  $-60$  mV.  $\text{Ca}^{2+}$  imaging was performed with a Nikon TS100-F inverted microscope (Nikon, Mississauga, ON, Canada) equipped with a Nikon Plan Fluor  $\times 20$ , 0.5 numerical aperture objective. The light source was a 75-W Xe arc lamp and a multiwavelength DeltaRAM V monochromatic illuminator (Photon Technology International/Horiba, London, ON, Canada) coupled to the microscope with a UV-grade liquid-light guide. Excitation wavelengths were 340 and 380 nm, which were controlled by a Windows-based computer, a Photon Technology International computer interface, and EasyRatio Pro software (v1.10; Photon Technology International). Emitted light passed through a 400-nm long-pass dichroic mirror and a 510/40-nm emission barrier filter before being detected by a Cool SNAP HQ2 charge-coupled device camera ( $696 \times 520$  pixels) (Photometrics, Tucson, AZ).

The ratio of the emission following 340- and 380-nm excitation (340/380) was taken to reflect free intracellular  $\text{Ca}^{2+}$  (29) and was sampled every 10 s from a region of interest defined over the soma and averaged 4–8 frames per acquisition. Camera gain was maximized, pixel binning set at 2, and exposure time at each wavelength fixed to 1 s. The camera intensifier voltage was set based on the initial fluorescence intensity of a neuron at the start of the experiment and maintained constant thereafter. Image acquisition, emitted light sampling, and ratio calculations were performed with EasyRatio Pro.

### Reagents and Drug Application

The culture dish served as the bath and, before the start of an experiment, solution exchanges were accomplished by using a calibrated transfer pipette to replace the tcASW with  $\text{Ca}^{2+}$ - $\text{Cs}^+$ -TEA ASW or nASW. In most cases, drugs were introduced before or during recording by removing  $\leq 20$   $\mu\text{L}$  of saline from the bath, mixing it with 2–8  $\mu\text{L}$  of drug stock solution, and then introducing that mixture back into the bath. Care was taken to pipette near the side of the dish and as far away as possible from the neuron. Exceptions were  $\text{Zn}^{2+}$  and sometimes  $\text{Co}^{2+}$ , which were superfused, as well as acetylcholine, which was either pressure-ejected or superfused. For superfusion, a square-barreled,  $\sim 500$ - $\mu\text{m}$ -bore glass pipette (8250, VitroCom, Mountain Lakes, NJ) was positioned with a micromanipulator 300–500  $\mu\text{m}$  from the soma. This pipette continuously flowed extracellular saline over the neuron, which was switched to drug-containing saline by activating a stopcock to select between various gravity-driven reservoirs. For pressure ejection, a PMI-200 pressure ejector (Dagan, Minneapolis, MN) delivered 2-s, 75- to 100-kPa pulses to an unpolished whole cell pipette (1- to 2- $\mu\text{m}$  tip diameter) filled with 1 mM acetylcholine (in nASW) and positioned  $\sim 50$   $\mu\text{m}$  away from the soma.

Water was used to dissolve the following as stocks at the indicated concentrations: acetylcholine (10 or 100 mM; A6625, Sigma-Aldrich),  $\text{Co}^{2+}$  (1 M,  $\text{CoCl}_2 \cdot 6\text{H}_2\text{O}$ ; C2911, Sigma-Aldrich),  $\text{Ni}^{2+}$  (1 M,  $\text{NiCl}_2 \cdot 6\text{H}_2\text{O}$ ; N6136, Sigma-Aldrich), verapamil (100 mM; V4629, Sigma-Aldrich), and  $\omega$ -conotoxin G1Va (1 mM; SNX124, Alomone, Jerusalem, Israel). Because of solubility issues,  $\text{Zn}^{2+}$  ( $\text{ZnCl}_2$ ; 211273, Sigma-Aldrich) solutions were made in  $\text{Ca}^{2+}$   $\text{Cs}^+$ -TEA or nASW at the desired concentration just before experiments. DMSO was used to dissolve phorbol 12-myristate 13-acetate (PMA, 10 mM; 79346, Sigma-Aldrich).

### Analysis

For all analyses, two cursors were placed apart at designated times on a trace (see below) before a voltage pulse or drug addition, and the average between the cursors served as a baseline. The peak or average of the response was measured by placing an additional two cursors on either side of the peak or a steady-state region. Clampfit then calculated the peak or average amplitude relative to baseline. In most cases, current was normalized to cell size by dividing by the whole cell capacitance (obtained from the EPC-8 whole cell capacitance compensation circuitry).

The current-voltage relationship ( $I/V$ ) of the rapid  $\text{Ca}^{2+}$  current was ascertained by measuring the peak current relative to a 3-ms baseline region at  $-60$  mV, 0.5 ms before the 200-ms, 10-mV increment steps from  $-60$  to  $+60$  mV. After the protocol was run once, it was delivered a second time in

the presence of select divalent metals ( $\text{Ni}^{2+}$ ,  $\text{Co}^{2+}$ ,  $\text{Zn}^{2+}$ ) or verapamil at various concentrations. The step from  $-60$  to  $+10$  mV, which evoked the largest  $\text{Ca}^{2+}$  current (see RESULTS for details), was used to normalize to the current before and after antagonist application in the same cell, which was later plotted against antagonist concentration. The concentration-response curve was fit with an asymmetric sigmoidal, five-parameter logistic equation in Prism (v9; GraphPad Software, San Diego, CA) to provide the Hill coefficient ( $n_H$ ; a measure of ligand cooperativity) and both the  $\text{IC}_{50}$  and  $\text{IC}_{100}$  (the concentration required to halve and eliminate the maximal current, respectively), where  $X$  is  $\log_{10}$  concentration of drug and  $\log Xb$  is the inflection point defined by  $\log \text{IC}_{50}$  and symmetry parameter  $S$ :

$$\% \text{ specific binding} = \frac{\text{top} - \text{bottom}}{1 + 10^{[(\log Xb - x) \cdot n_H]^S}}$$

$$\log Xb = \log \text{IC}_{50} + \left(\frac{1}{n_H}\right) \left(\log 2^{\frac{1}{S}} - 1\right)$$

The effect of  $\text{Co}^{2+}$ ,  $\text{Zn}^{2+}$ , or verapamil at the  $\text{IC}_{50}$  on rapid  $\text{Ca}^{2+}$  current activation was determined by dividing the peak current elicited at each voltage step by the current at  $+10$  mV, i.e., the maximum current. This was averaged across cells at a given step voltage and fit with the Boltzmann equation in Prism. The Boltzmann fit provided the half-maximal voltage ( $V_{1/2}$ ) of activation (the voltage required to recruit half of the maximum current) and the slope factor ( $k$ ; the amount of voltage required to change the current  $e$ -fold).

$$G(S) = \text{bottom} + \frac{(\text{top} - \text{bottom})}{1 + \exp\left(\frac{V_{1/2} - x}{k}\right)}$$

Persistent  $\text{Ca}^{2+}$  current was evoked by delivering 10-s steps from  $-50$  to  $-20$  mV in 10-mV increments. Offline leak subtraction involved subtracting currents not blocked by the  $\text{IC}_{100}$  of the  $\text{Ca}^{2+}$  current blockers,  $\text{Co}^{2+}$ ,  $\text{Ni}^{2+}$ , verapamil, and  $\text{Zn}^{2+}$ , from currents evoked under control conditions. For analysis of the leak-subtracted traces,  $\sim 150$  ms of baseline was averaged  $\sim 12$  ms before the step, whereas the last  $\sim 1$  s of the steps,  $\sim 50$  ms before the offset, was averaged for  $\text{Ca}^{2+}$  current. The difference between the averaged current during the step and the baseline was taken as the persistent current.

Peak amplitude of the acetylcholine-evoked depolarization or current was derived from response to superfusion of 1 mM acetylcholine for 5 s or pressure ejection of 1 mM acetylcholine for 2 s. To quantify the peak acetylcholine-evoked depolarization or current,  $\sim 10$  s of baseline membrane potential or current was averaged  $\sim 500$  ms before the response onset. The maximal amplitude of the response was taken as the difference between this average baseline and the peak depolarization or current. The desensitization of acetylcholine-induced current under voltage clamp was expressed as a percentage of current remaining by dividing the second acetylcholine-evoked current by the first within the same neuron. For responses recorded under current clamp that presented with robust spiking, which made the peak depolarization difficult to visualize, Clampfit was used to generate an all-points histogram at the depolarized potentials of the response. The largest peak of the histogram was fit

in Clampfit with a Gaussian function by the least-squares method and a simplex search and taken as the average membrane potential during the firing period, with the difference versus baseline (obtained as above) being the depolarization amplitude. To determine firing frequency in acetylcholine, the number of spikes during the response was calculated with the Clampfit threshold search function and divided by the total time of the burst.

For analysis of intracellular  $\text{Ca}^{2+}$ , Origin (v7; OriginLab, Northampton, MA) was used to import and plot ImageMaster Pro files as line graphs. The 1 min before response onset was averaged and served as baseline, and peak was measured relative to the baseline.  $\text{Ca}^{2+}$  influx evoked by the waveforms (see RESULTS for details) was quantified by calculating the peak 340/380 versus the prestimulus baseline. Change was expressed as a percent change of the new ratio over the baseline ratio.

Summary data are presented as means in line or bar graphs with error bars representing standard deviation. Statistical analysis was performed with InStat (v3.1; GraphPad Software) or Prism. The Kolmogorov–Smirnov method was used to test data sets for normality. If the data were normal, Student's unpaired  $t$  test with the Welch correction was used to determine the differences between two means. If the data were not normally distributed, the Mann–Whitney  $U$  test was used. Comparison between multiple means was performed with an ordinary one-way analysis of variance (ANOVA) and the Dunnett multiple comparisons post hoc test (for normally distributed data) or a Kruskal–Wallis one-way ANOVA with Dunn's multiple comparisons test (for not normally distributed data). All statistical comparisons were two tailed, and means were considered significantly different if the  $P$  value was  $< 0.05$ . When possible, as per the output of the software, exact  $P$  values are reported. The  $n$  values reported in the text indicate number of neurons;  $n$  values are also provided within the bars of all summary data graphs.

## RESULTS

### Brief Cholinergic Current Evokes a Prolonged Depolarization in Bag Cell Neurons

Single bag cell neurons in primary culture were recorded under sharp-electrode current clamp or whole cell voltage clamp using  $\text{Na}^+$ -based normal artificial sea water (nASW) as extracellular saline (Fig. 1, right inset). Sharp electrodes were filled with a  $\text{K}^+$ -acetate-based saline, whereas whole cell electrodes were filled with a  $\text{K}^+$ -aspartate-based intracellular saline (see *Whole Cell Voltage-Clamp Recordings* and *Sharp-Electrode Current-Clamp Recordings* for details). A 2-s pressure ejection of 1 mM acetylcholine onto neurons current-clamped at a resting potential of approximately  $-60$  mV evoked spiking and a prolonged depolarization of 30–50 mV lasting  $\leq 8$  min ( $n = 7$ ) (Fig. 1, top). However, the same application of acetylcholine onto different neurons whole cell voltage-clamped to  $-60$  mV resulted in a much more short-lived inward current that peaked between  $-10$  and  $-20$  nA and lasted  $\sim 1.5$  min ( $n = 6$ ) (Fig. 1, bottom). This difference in duration was significant, with the depolarization presenting an  $\sim 165$ -s time to 75% recovery, compared with  $\sim 25$  s for the current (Fig. 1, left inset).

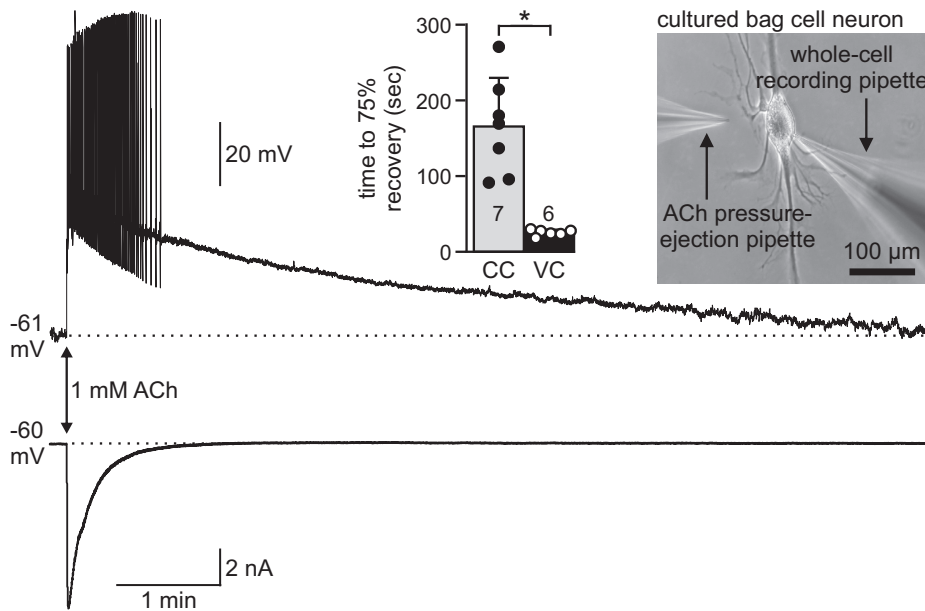


**Figure 1.** Cholinergic current and depolarization are kinetically distinct. Two separate cultured bag cell neurons are bathed in normal artificial seawater (nASW) and subjected to either sharp-electrode current clamp (CC) with a  $K^+$ -acetate-based pipette solution or whole cell voltage clamp (VC) with a  $K^+$ -Asp-based intracellular solution. *Top:* a 2-s pressure ejection (at arrow) of 1 mM acetylcholine (ACh) evokes depolarization and bursting from a resting potential of  $-61$  mV under current clamp. The response does not recover until the end of the trace ( $\sim 8$  min). *Bottom:* the same stimulus in a different neuron under voltage clamp at  $-60$  mV causes a transient inward current that fully recovers by  $\sim 1.5$  min. Timescale applies to both *top* and *bottom*. *Left inset,* the time to 75% recovery of the current is significantly faster than the depolarization ( $t_{5,75} = 6.06$ ;  $*P = 0.001$ ; unpaired Student's *t* test, Welch corrected). *Right inset,* a cultured bag cell neuron with a whole cell recording electrode and a pressure-ejection pipette. Numbers within the bars are *n* values that reflect number of neurons.

Given that the acetylcholine-induced current is not sensitive to metabotropic blockers (10) and does not conduct  $Ca^{2+}$  (26), it is likely that the depolarization produced by acetylcholine recruits a voltage-dependent mechanism to further the response. Potential candidates are voltage-gated  $Ca^{2+}$  channels, which rapidly activate upon membrane depolarization but can remain open on a longer timescale as the channel transitions between opening and closing, creating a “window current” (27, 30, 31). Thus, we examined the pharmacology and physiology of the  $Ca^{2+}$  current to find a suitable blocker(s) that could be used to test the role of  $Ca^{2+}$  current in acetylcholine-induced depolarization.

### Rapid-Onset, Voltage-Gated $Ca^{2+}$ Currents in Bag Cell Neurons

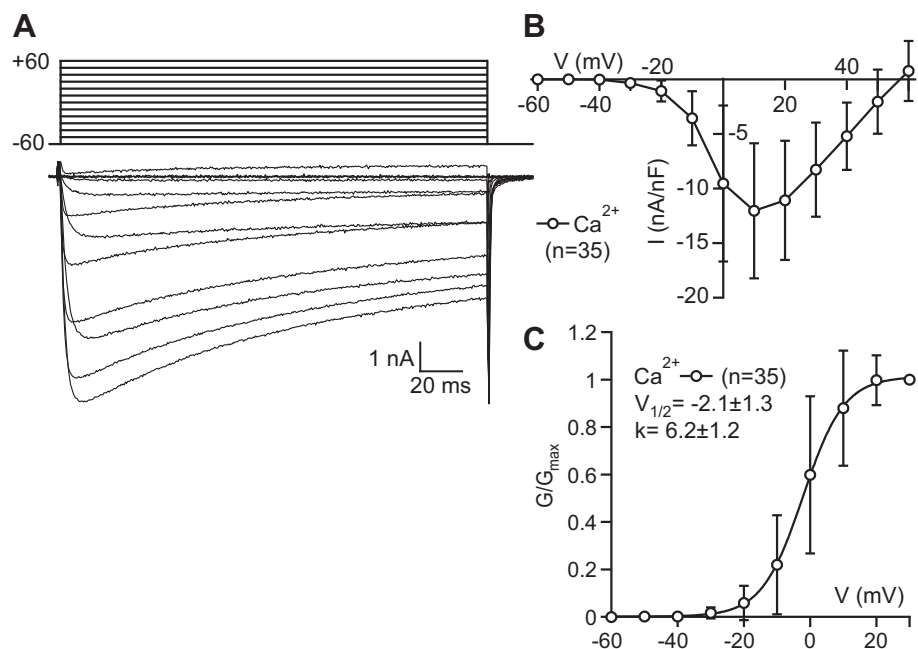
On a structural basis, bag cell neuron voltage-gated  $Ca^{2+}$  channels most closely resemble vertebrate L-type channels (32); accordingly, the current presents slow inactivation and partial sensitivity to micromolar concentrations of nifedipine (16, 33) as well as full block with millimolar concentrations of  $Ni^{2+}$  (12). To demonstrate this current, whole cell voltage clamp in  $Ca^{2+}$ - $Cs^+$ -TEA ASW external with  $Cs^+$ -Asp intracellular solution was used (see *Whole Cell Voltage-Clamp Recording* for details). Delivering 200-ms, 10-mV incremental steps from  $-60$  to  $+60$  mV evoked rapid-onset, but relatively slow-inactivating  $Ca^{2+}$  currents in the nano-ampere range ( $n = 35$ ) (Fig. 2A). Normalizing the peak current to cellular capacitance and plotting against voltage produced a U-shaped relationship of current density versus membrane potential, with an onset between  $-30$  and  $-40$  mV, a reversal at approximately  $+60$  mV, and a maximum current density of  $\sim 12$  nA/nF at  $+10$  mV ( $n = 35$ ) (Fig. 2B), like earlier reports (12, 27). Normalizing the conductance to the maximum at  $+30$  mV and fitting with a Boltzmann equation revealed a  $V_{1/2}$  at approximately  $-2$  mV with a slope factor of  $\sim 6$  (Fig. 2C). Maximum current density was at  $+10$  mV, whereas the conductance plateaued at  $+30$  mV.

### Rapid-Onset, Voltage-Gated $Ca^{2+}$ Currents Are Sensitive to $Co^{2+}$ , $Zn^{2+}$ , and Verapamil

We previously established  $Ni^{2+}$  as a  $Ca^{2+}$  channel blocker in bag cell neurons (12). However, to have more pharmacological tools for testing the role of  $Ca^{2+}$  channels in the acetylcholine-induced depolarization, we assayed  $Co^{2+}$ ,  $Zn^{2+}$ , and verapamil, which have been used to block  $Ca^{2+}$  channels in other *Aplysia* neurons (34–36). The ultimate goal was to find a  $Ca^{2+}$  channel blocker that could be applied during the voltage response to acetylcholine without directly affecting the cholinergic receptor. Hence, neurons were whole cell voltage-clamped at  $-60$  mV and given a step to  $+10$  mV for 100 or 200 ms before and after the introduction of  $Co^{2+}$  (Fig. 3A),  $Zn^{2+}$  (Fig. 3C), or verapamil (Fig. 3E) at different concentrations.  $Co^{2+}$  and verapamil were bath applied, whereas  $Zn^{2+}$  was superfused because of solubility issues involving precipitation at concentrations  $>1$  mM, precluding the use of stock solutions (see *Reagents and Drug Application* for details).

After blocker addition, the  $Ca^{2+}$  currents were reduced but still rapid in activation and slow in inactivation, unless the drugs were at their highest concentration, during which the current essentially remained at baseline. The peak current in the presence of a given blocker was normalized to that of control, plotted against blocker concentration, and fit with an asymmetric sigmoidal equation (Fig. 3, B, D, and F) (see *Analysis* for details). Fitting these concentration-inhibition curves provided  $IC_{50}$  values of  $\sim 1$  mM for  $Co^{2+}$  and  $\sim 300$   $\mu$ M for both  $Zn^{2+}$  and verapamil, which were in agreement with the effective concentrations observed in certain vertebrate cells (37–39). Those same fits also yielded Hill coefficients that reflected the cooperativity a given blocker exhibited while inhibiting the channel. Both  $Co^{2+}$  and verapamil, with Hill coefficients of  $-2.8$  and  $-1.4$ , respectively, showed positive cooperativity, where the binding of one ion or molecule increased the binding affinity of additional blocker. Conversely,  $Zn^{2+}$

**Figure 2.** Rapid, voltage-dependent  $\text{Ca}^{2+}$  currents in bag cell neurons. **A:** a neuron is whole cell voltage clamped in  $\text{Ca}^{2+}$ - $\text{Cs}^+$ -tetraethylammonium artificial seawater with  $\text{Cs}^+$ -Asp intracellular solution to isolate  $\text{Ca}^{2+}$  currents. From a holding potential of  $-60$  mV, 200-ms steps to  $+60$  mV in 10-mV increments (top) evoke rapid-onset, voltage-dependent  $\text{Ca}^{2+}$  current (bottom). Capacitance artifact at onset is truncated for display. **B:** summary of peak current ( $I$ ) normalized to capacitance and plotted against the step voltages ( $V$ ) from **A**. Onset is  $-30$  mV, with peak at  $+10$  mV and reversal of  $+57.5$  mV. **C:** summary of conductance normalized to maximal ( $G/G_{\text{max}}$ ) at  $+30$  mV and plotted against step voltage. Conductance was derived from peak current divided by the driving force, i.e., step voltage minus reversal potential.  $V_{1/2}$  indicates the voltage at which conductance is half-maximum, and  $k$  reflects the slope factor.



had negative cooperativity, with a Hill coefficient of  $-0.8$ , which indicated that initial binding of the ion led to reduced binding affinity of more blocker.

### $\text{Co}^{2+}$ , $\text{Zn}^{2+}$ , or Verapamil Block of $\text{Ca}^{2+}$ Current Is Not Voltage Dependent

For  $\text{Ca}^{2+}$  current blockers to be effective for our purposes, they must have the same antagonistic effects even during depolarized potentials; as such, rapid  $\text{Ca}^{2+}$  currents were again evoked with our standard 200-ms steps from  $-60$  to  $+60$  mV. In the presence of the  $\text{IC}_{100}$  of  $\text{Ni}^{2+}$  [10 mM; concentration taken from Hung and Magoski (12); used here as a positive control] ( $n = 9$ ),  $\text{Co}^{2+}$  (4 mM) ( $n = 5$ ),  $\text{Zn}^{2+}$  (1 mM) ( $n = 6$ ), or verapamil (1 mM) ( $n = 4$ ), block was largely complete with only residual current remaining, although  $\text{Zn}^{2+}$  sometimes presented voltage-dependent relief (Fig. 4A). When peak  $\text{Ca}^{2+}$  current was plotted against step voltage, all four blockers gave some steady inhibition regardless of membrane potential (Fig. 4B). To examine the impact of block on voltage dependence, current-voltage relationships were made in the presence of the  $\text{IC}_{50}$  of each drug and the  $\text{Ca}^{2+}$  current was normalized to the maximal current at  $+10$  mV, plotted against step voltage, and fit with the Boltzmann equation to obtain activation curves (see Analysis for details). Compared with a control  $V_{1/2}$  of 9–12 mV ( $n = 6$ –14), the activation curve in  $\text{Co}^{2+}$  was shifted to the right by  $\sim 10$  mV ( $n = 10$ ) (Fig. 4C) and that in verapamil was moderately shifted to the left by  $\sim 4$  mV ( $n = 14$ ) (Fig. 4D), whereas  $\text{Zn}^{2+}$  ( $n = 6$ ) had even smaller effects on activation, with a right shift of  $< 3$  mV (Fig. 4E). Thus, the  $\text{IC}_{50}$  of  $\text{Co}^{2+}$ , and to a smaller extent  $\text{Zn}^{2+}$ , resulted in less  $\text{Ca}^{2+}$  current during a given depolarization compared with control; the opposite was the case for verapamil. That stated, these effects on voltage dependence were relatively minimal, considering that the  $\text{IC}_{100}$  of each blocker substantially reduced the current at all voltages.

### $\text{Cd}^{2+}$ and $\omega$ -Conotoxin GIVa Are Ineffective $\text{Ca}^{2+}$ Current Blockers

We also looked at  $\text{Cd}^{2+}$ , another divalent metal, and  $\omega$ -conotoxin GIVa, a 27-amino acid peptide produced by *Conus geographus*, as candidate blockers because they have been widely used to suppress L-type (40–43) and N-type (44–47) channels in amphibian, avian, mammalian, and/or molluscan cells. In *Aplysia*,  $\text{Cd}^{2+}$  inhibits voltage-dependent  $\text{Ca}^{2+}$  current in L10 (48) and sensory neurons (49), whereas  $\omega$ -conotoxin inhibits buccal neuron  $\text{Ca}^{2+}$  current and transmitter release (50, 51).

We tested both blockers on  $\text{Ca}^{2+}$  currents evoked by 200-ms steps from  $-60$  to  $+40$  mV or  $+60$  mV in 10-mV increments. At 700  $\mu\text{M}$ , the amount of block by  $\text{Cd}^{2+}$  ( $n = 2$ ) was very modest (Fig. 5A, inset). Moreover,  $\text{Cd}^{2+}$  appeared to be toxic, as a concentration of 900  $\mu\text{M}$  produced only an outward current at all tested voltages except for the maximum step at  $+40$  mV (not shown). In addition, cumulative applications of the metal, from 100  $\mu\text{M}$  to 3 mM, in nASW to a cell dialyzed with  $\text{K}^+$ -Asp intracellular solution at a holding potential of  $-60$  mV led to a rapid increase in holding current and cell death (Fig. 5A). With respect to  $\omega$ -conotoxin ( $n = 10$ ), a concentration of 8  $\mu\text{M}$ , based on Trudeau et al. (50) and Fossier et al. (51), was added to the bath  $\sim 30$  min before recording. However, peak  $\text{Ca}^{2+}$  currents normalized to capacitance showed little difference from control ( $n = 9$ ), albeit the  $I/V$  was shifted to the right (Fig. 5B). The activation curve in  $\omega$ -conotoxin was right-shifted by  $\sim 7.5$  mV versus control when fit with a Boltzmann equation (Fig. 5C).

### Persistent Voltage-Gated $\text{Ca}^{2+}$ Current Is Revealed by $\text{Ca}^{2+}$ Blocker and Leak Subtraction

Having established  $\text{Co}^{2+}$ ,  $\text{Zn}^{2+}$ , and verapamil as effective blockers of rapid current, we next determined whether they could successfully reveal persistent  $\text{Ca}^{2+}$  currents. Our earlier work using  $\text{Ni}^{2+}$  block subtraction showed that  $\text{Ni}^{2+}$  is capable of eliminating persistent  $\text{Ca}^{2+}$  currents (27), so we also

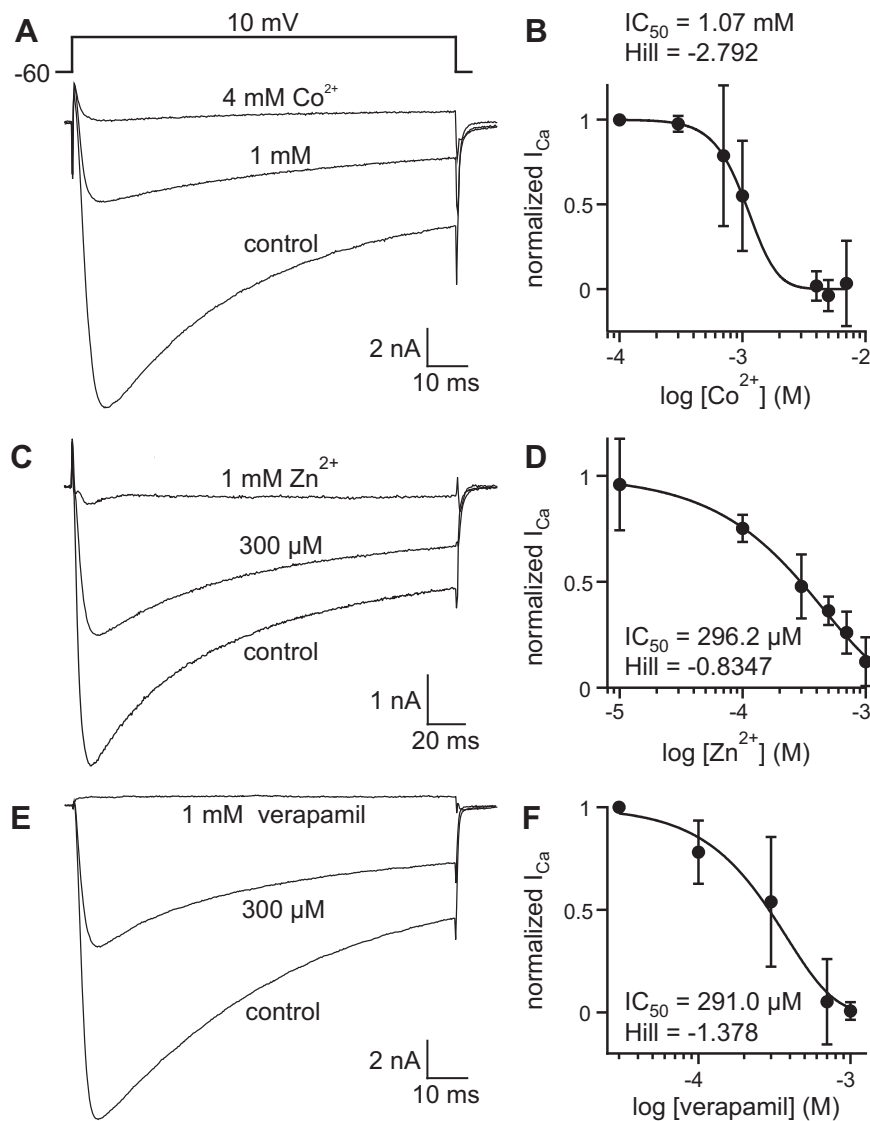


**Figure 3.**  $\text{Co}^{2+}$ ,  $\text{Zn}^{2+}$ , or verapamil reduce the  $\text{Ca}^{2+}$  current in a concentration-dependent manner. *A*, *C*, and *E*: separate bag cell neurons are voltage-clamped at  $-60$  mV in  $\text{Ca}^{2+}$ - $\text{Cs}^{+}$ -tetraethylammonium artificial seawater with  $\text{Cs}^{+}$ -Asp intracellular solution and given a step to  $+10$  mV for 100 or 200 ms. The step is repeated in the presence of  $\text{Co}^{2+}$  (*A*),  $\text{Zn}^{2+}$  (*C*), or verapamil (*E*) at the indicated concentrations.  $\text{Zn}^{2+}$  is tested at 1 concentration per cell.  $\text{Co}^{2+}$  or verapamil is added incrementally, with a saturating concentration always being added at the end after some combination of lower concentrations. Order of potency is:  $\text{Co}^{2+} > \text{Zn}^{2+} > \text{verapamil}$ . *B*, *D*, and *F*:  $\text{Co}^{2+}$  (*B*),  $\text{Zn}^{2+}$  (*D*), and verapamil (*F*) dose-response curves. Peak current ( $I_{\text{Ca}}$ ) evoked in  $\text{Co}^{2+}$ ,  $\text{Zn}^{2+}$ , or verapamil is divided by the corresponding control current, plotted against the applied concentration, and fit with an asymmetric sigmoidal curve to obtain the  $\text{IC}_{50}$  and Hill coefficient.

employed it here for comparison. Neurons were voltage-clamped at  $-60$  mV and stimulated for 10 s in 10-mV increments from  $-50$  to  $-20$  mV before and after delivery of the  $\text{IC}_{100}$  of  $\text{Ni}^{2+}$ ,  $\text{Co}^{2+}$ ,  $\text{Zn}^{2+}$ , or verapamil. Leak was eliminated by subtracting the voltage steps delivered after block by 10 mM  $\text{Ni}^{2+}$  ( $n = 20$ ), 4 mM  $\text{Co}^{2+}$  ( $n = 16$ ), 1 mM  $\text{Zn}^{2+}$  ( $n = 8$ ), or 1 mM verapamil ( $n = 8$ ) (Fig. 6, *A–D*) (see Analysis for details). Leak subtraction revealed a small, inward, voltage-dependent current of hundreds of picoamperes that stabilized by the end of each step. Hence, mean current over the last 1 s of the step was measured as persistent current.  $\text{Ni}^{2+}$  revealed the greatest persistent  $\text{Ca}^{2+}$  current, which was significantly higher in amplitude than current after  $\text{Co}^{2+}$ ,  $\text{Zn}^{2+}$ , or verapamil block subtraction at  $-50$  and  $-40$  mV (Fig. 6*E*). At  $-30$  mV, current after  $\text{Ni}^{2+}$  subtraction was significantly greater than that after  $\text{Co}^{2+}$  or  $\text{Zn}^{2+}$  but not verapamil.

### Cholinergic-like Waveforms Cause Voltage-Dependent $\text{Ca}^{2+}$ Influx

If the acetylcholine-induced depolarization is prolonged by evoking voltage-dependent  $\text{Ca}^{2+}$  current, a waveform

mimicking the voltage changes during an acetylcholine response should activate the  $\text{Ca}^{2+}$  channel. We created waveforms based on typical cholinergic depolarizations and delivered them under voltage clamp, instead of applying acetylcholine under current clamp, so to avoid any confounding action potential firing. Voltage commands were categorized into two, distinct waveforms: *waveform 1* and *waveform 2*, and were modeled from prior sharp-electrode current-clamp recordings of acetylcholine-evoked membrane potential changes (10, 28). Essentially, these waveforms represented two commonly observed responses to acetylcholine under physiological conditions, with *waveform 1* depicting a less protracted response than *waveform 2*. From a holding potential of  $-60$  mV, *waveform 1* changed the membrane potential to  $-30$  mV over 5 s, to  $-26$  mV over 2 s, to  $-51$  mV over 75 s, and to  $-58$  mV over 18 s (Fig. 7*A*, top). *Waveform 2* also started at  $-60$  mV, then to  $-20$  mV over 2 s, to  $-35$  mV over 150 s, and to  $-53$  mV over 225 s (Fig. 7*B*, top). In either case, only the continuous changes in membrane voltage without action potentials were modeled.

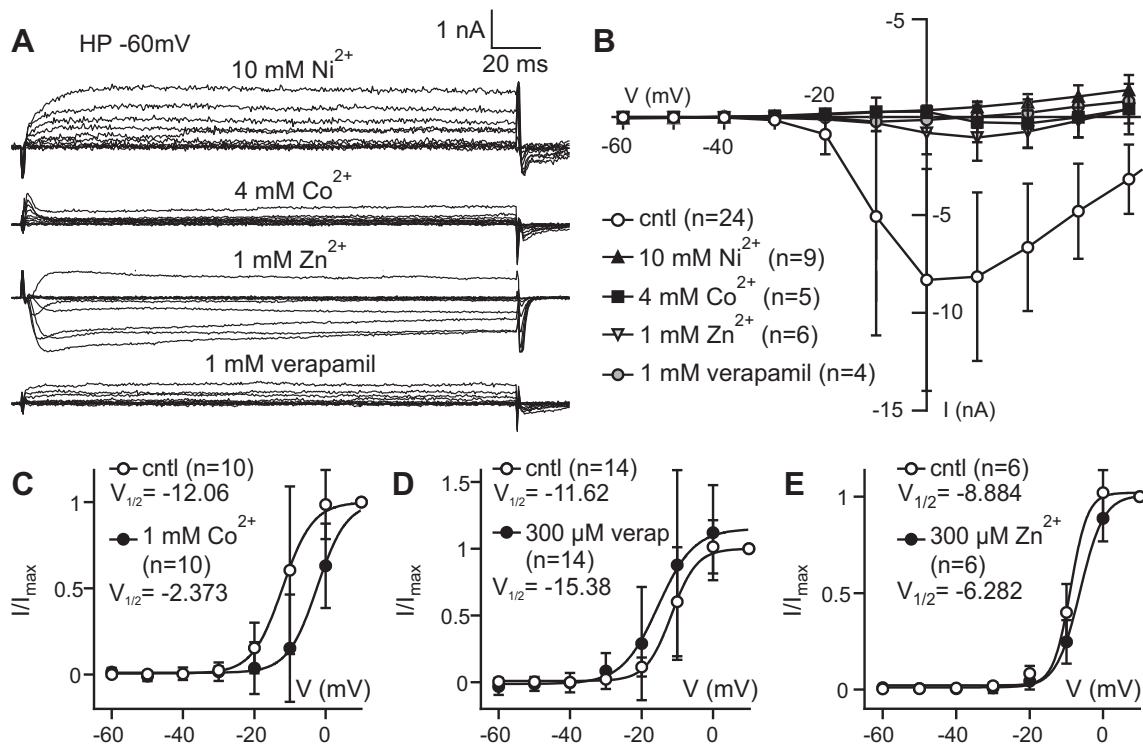


**Figure 4.** Effect of select divalent metals or verapamil on  $\text{Ca}^{2+}$  current voltage dependence. **A:**  $\text{Ca}^{2+}$  currents from separate neurons evoked by 200-ms pulses from  $-60$  mV [holding potential (HP)] to  $+60$  mV in  $10$ -mV increments while exposed to the  $\text{IC}_{100}$  (concentration required to eliminate maximal current) of  $\text{Ni}^{2+}$  (top;  $10$  mM),  $\text{Co}^{2+}$  (top middle;  $4$  mM),  $\text{Zn}^{2+}$  (bottom middle;  $1$  mM), or verapamil (bottom;  $1$  mM). Capacitance artifacts are truncated for display. Scale bars apply to all traces. **B:** average peak  $\text{Ca}^{2+}$  current ( $I$ ) plotted against step voltage ( $V$ ), along with all parallel control currents pooled for comparison. The divalent metals and verapamil cause a complete or a near-complete block with no observable voltage dependence to the inhibition, except to a small extent with  $\text{Zn}^{2+}$ . **C–E:** activation curves of  $\text{Ca}^{2+}$  current under control conditions and in the presence of the  $\text{IC}_{50}$  of  $\text{Co}^{2+}$  ( $1$  mM; **C**), verapamil ( $300$   $\mu\text{M}$ ; **D**), or  $\text{Zn}^{2+}$  ( $300$   $\mu\text{M}$ ; **E**). The activation curve in  $\text{Co}^{2+}$  is shifted to the right compared with control, as indicated by the more positive half-maximal voltage of activation ( $V_{1/2}$ ). Conversely, the activation curve in verapamil is shifted moderately to the left vs. control, as indicated by the more negative  $V_{1/2}$ . The impact of  $\text{Zn}^{2+}$  on activation is negligible.  $I/I_{\text{max}}$ ,  $\text{Ca}^{2+}$  current normalized to maximal current (at  $+10$  mV).

Neurons were voltage-clamped to  $-60$  mV in  $\text{Ca}^{2+}$ - $\text{Cs}^{+}$ -TEA ASW extracellular solution and dialyzed with  $\text{Cs}^{+}$ -Asp-based intracellular solution. Both waveforms evoked a rapid-onset, long-duration inward  $\text{Ca}^{2+}$  current of several nanoamperes, which was revealed by subtracting leak current following a block with  $\text{Co}^{2+}$  at the  $\text{IC}_{100}$  of  $4$  mM. However, *waveform 1* ( $n = 7$ ) (Fig. 7A, bottom) resulted in a faster inactivation than *waveform 2* ( $n = 5$ ) (Fig. 7B, bottom) because of shorter total duration at depolarized membrane potentials. Therefore, although peak current density between the two waveforms was not different ( $\sim 1$  nA/nF for both), *waveform 2* had a significantly greater total  $\text{Ca}^{2+}$  influx, measured as area above the curve, at  $\sim 40$  nCb/nF, compared to *waveform 1* at  $\sim 20$  nCb/nF (Fig. 7C). That the more protracted *waveform 2* yielded a larger response was consistent with total  $\text{Ca}^{2+}$  influx being a function of the voltage integral.

As a more physiological assessment of  $\text{Ca}^{2+}$  influx, neurons were maintained in nASW and loaded with the  $\text{Ca}^{2+}$ -sensitive dye fura PE3 in  $\text{K}^{+}$ -Asp-based intracellular solution under whole cell voltage clamp at  $-60$  mV. *Waveforms 1* and *2* were delivered to the same cell sequentially ( $n = 4$ ) while ratiometrically imaging for intracellular  $\text{Ca}^{2+}$  (see *Ca<sup>2+</sup> Imaging* for details). Both waveforms caused a sharp increase in fluorescence (Fig. 7D), but *waveform 2*, with an

$\sim 20\%$  increase, had a larger change in peak fluorescence than *waveform 1*, with an  $\sim 5\%$  increase (Fig. 7E).

#### The Acetylcholine-Induced Current Is Not Affected by $\text{Zn}^{2+}$ or $\text{Co}^{2+}$ at the $\text{IC}_{50}$

Given that the select  $\text{Ca}^{2+}$  channel blockers can reveal persistent  $\text{Ca}^{2+}$  current, we examined whether they interact with the acetylcholine-induced current and exhibit confounding antagonism. Since our earlier work showed that the acetylcholine-induced current desensitizes with repeated applications (10), acetylcholine was pressure-ejected twice at  $1$  mM for  $2$  s with an interval of  $10$  min (see *Reagents and Drug Application* for details) to observe the effects before and after the introduction of blockers. Desensitization was expressed as a percentage of current remaining at the second versus the first application.  $\text{Ni}^{2+}$ , verapamil, or  $\text{Co}^{2+}$  was added directly to the bath after the first acetylcholine-induced current recovered to baseline. As a positive control, some neurons were exposed to hexamethonium, an ionotropic acetylcholine receptor antagonist previously shown to suppress acetylcholine-induced currents in bag cell neurons (10). Again, because of solubility issues,  $\text{Zn}^{2+}$  was superfused over the cell with or without acetylcholine. The extent of desensitization compared with control pairs of applications was taken as an effect of a given  $\text{Ca}^{2+}$  channel blocker on the acetylcholine receptor.

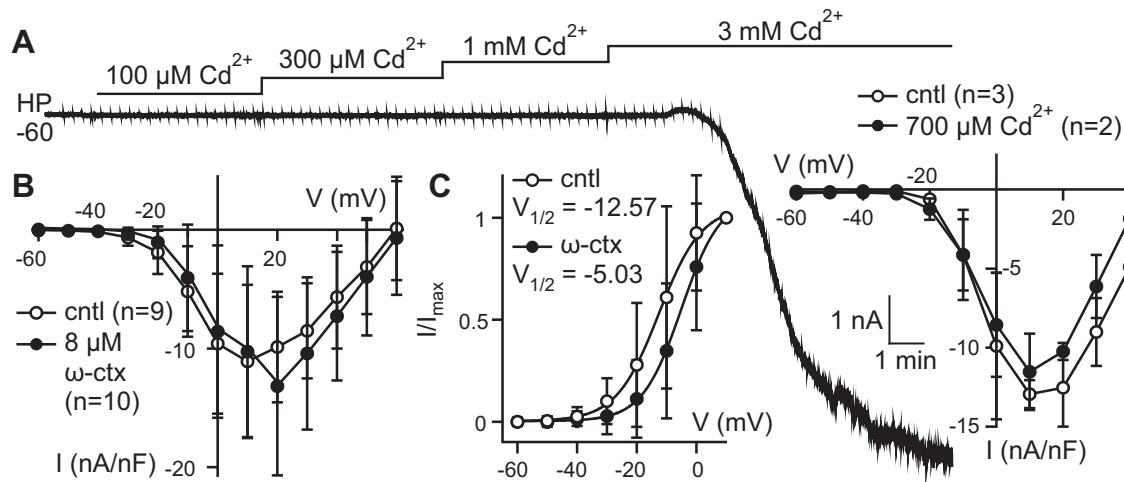


**Figure 5.**  $\text{Cd}^{2+}$  and  $\omega$ -conotoxin GIVA ( $\omega$ -ctx) are ineffective  $\text{Ca}^{2+}$  current blockers. **A:** a bag cell neuron is dialyzed with  $\text{Cs}^+$ -Asp-based intracellular solution, voltage-clamped at  $-60$  mV [holding potential (HP)], and exposed to cumulative doses of  $\text{Cd}^{2+}$  (at steps) in  $\text{Ca}^{2+}$ - $\text{Cs}^+$ -tetraethylammonium artificial seawater;  $3$  mM resulted in a marked increase in holding current ( $n = 4$ ). *Inset*, at an intermediate concentration of  $700 \mu\text{M}$   $\text{Cd}^{2+}$  weakly inhibits the current density (nA/nF). **B:** summary of peak  $\text{Ca}^{2+}$  current normalized to capacitance and plotted against step voltage in control or neurons pretreated with  $8 \mu\text{M}$   $\omega$ -ctx. Peak  $\text{Ca}^{2+}$  current density in the presence of  $\omega$ -ctx (●) is similar to control (○), although the maximum current is shifted to the right. **C:** activation curves of the  $\text{Ca}^{2+}$  current in the absence and presence of  $\omega$ -ctx. Current is normalized to that at  $+10$  mV ( $I/I_{\text{max}}$ ), plotted against step voltage, and fit with a Boltzmann function. The activation curve in conotoxin is shifted to the right as indicated by the more positive half-maximal voltage of activation ( $V_{1/2}$ ).

The current was immediate in onset upon acetylcholine application, ranged typically between 1 and 20 nA, and decayed over  $\leq 1$  min for both the first and second applications. Under control conditions, without any antagonists added to the bath,  $\sim 60\%$  current remained at the second application ( $n = 17$ ) (Fig. 8, A and F). At  $500 \mu\text{M}$ , hexamethonium ( $n = 8$ ) blocked most of the second acetylcholine current (Fig. 8, B and F), whereas the  $\text{IC}_{50}$  of  $\text{Ni}^{2+}$  ( $1.5$  mM) ( $n = 5$ ) and verapamil ( $300 \mu\text{M}$ ) ( $n = 7$ ) left  $\sim 20\%$  and  $30\%$ , respectively, of the current remaining (Fig. 8, C, D, and F), which was a significantly greater drop than control, indicating block of the receptor. However, the amount of current remaining in the presence of the  $\text{IC}_{50}$  of  $\text{Co}^{2+}$  ( $1$  mM) ( $n = 6$ ) or  $\text{Zn}^{2+}$  ( $300 \mu\text{M}$ ) ( $n = 8$ ) (Fig. 8, E and G) was not significantly different from control, although the  $\text{IC}_{100}$  of  $\text{Co}^{2+}$  ( $4$  mM) ( $n = 9$ ) did cause some block resulting in a  $40\%$  remaining current (Fig. 8, F and H). All second currents in the presence of antagonists had similar inactivation duration as the first, except for verapamil, in which a rapid return to baseline after reaching a peak current was observed.

### The Acetylcholine-Induced Depolarization Is Sustained by Persistent $\text{Ca}^{2+}$ Current

Since the  $\text{IC}_{50}$  of  $\text{Co}^{2+}$  and  $\text{Zn}^{2+}$  suppressed  $\text{Ca}^{2+}$  currents without affecting the acetylcholine-induced current, these metals were tested for an effect on the acetylcholine-induced depolarization with sharp-electrode current clamp in nASW.  $\text{Zn}^{2+}$  was promptly eliminated from further consideration because  $300 \mu\text{M}$  of this metal alone hyperpolarized neurons to approximately  $-80$  mV, followed by a subsequent plateau potential to approximately  $-20$  mV, and eventually killed them (not shown).  $\text{Zn}^{2+}$  has nonspecific effects on  $\text{K}^+$ ,  $\text{Na}^+$ , ligand-gated, and/or acid-sensing channels (52), which may explain the outcomes we found. Conversely, results with  $\text{Co}^{2+}$  proved to be more interpretable. We sequentially

superfused acetylcholine and  $\text{Co}^{2+}$  with an  $\sim 5$ -s gap to ensure that  $\text{Ca}^{2+}$  channel block would occur soon after the depolarization began but with as little overlap as possible, i.e., acetylcholine at  $1$  mM was delivered for  $5$  s, after which the blocker was superfused for the remainder of the experiment.

In control, brief superfusion of acetylcholine alone ( $n = 10$ ) caused a rapid depolarization, often accompanied by a burst of action potentials ( $6/10$ ), with a subsequent prolonged depolarization lasting  $>2$  min (Fig. 9, A, top). Yet, if  $1$  mM  $\text{Co}^{2+}$  was introduced shortly after acetylcholine washout ( $n = 8$ ), the duration of depolarization was markedly reduced (Fig. 9A, bottom). There was a significant difference between the time to  $75\%$  recovery with acetylcholine alone ( $\sim 110$  s) versus  $\text{Co}^{2+}$  following acetylcholine ( $\sim 60$  s) (Fig. 9B, top). Note that the initial acetylcholine-induced depolarization was not significantly different between acetylcholine-alone ( $n = 10$ ) and acetylcholine, then  $\text{Co}^{2+}$  ( $n = 8$ ) conditions ( $\sim 31$  vs.  $\sim 35$  mV) (Fig. 9B, bottom).

Prior work in our laboratory demonstrated that phorbol 12-myristate 13-acetate (PMA), which activates PKC (53), enhances the persistent  $\text{Ca}^{2+}$  in bag cell neurons (27). Therefore, we hypothesized that triggering PKC would boost the acetylcholine-induced depolarization. Neurons were either pretreated with PMA for  $\sim 20$  min or maintained in nASW before being pressure-ejected with  $1$  mM acetylcholine for  $2$  s. Under control conditions ( $n = 5$ ), the acetylcholine-induced depolarization returned to baseline by  $75\%$  in  $\sim 50$  s (Fig. 9, C, top, and D, top, ) but with PMA ( $n = 5$ ) the depolarization was prolonged and the same recovery required  $\sim 5$  min (Fig. 9, C, bottom, and D, top). Furthermore, whereas control neurons respond to acetylcholine with a burst of  $\sim 20$  action potentials, PMA amplified the response to  $\sim 140$  action potentials ( $n = 5$ ), which was a significant difference (Fig. 9D, bottom).

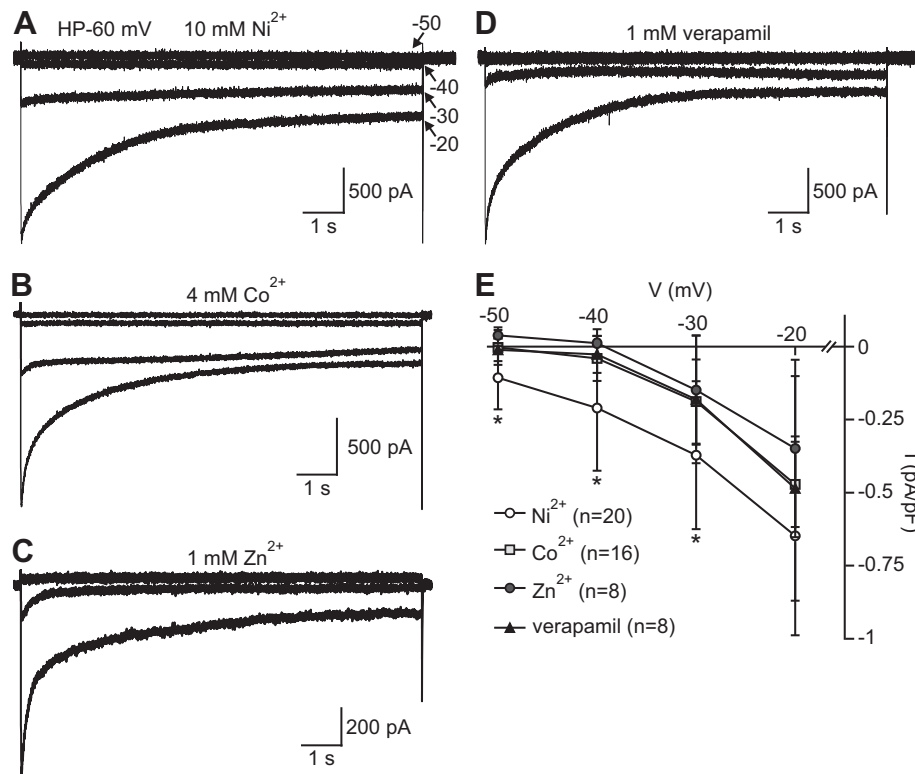


**Figure 6.** Persistent voltage-activated Ca<sup>2+</sup> current is revealed by select divalent metals or verapamil. *A–D*: applying the IC<sub>100</sub> (concentration required to eliminate maximal current) of Ni<sup>2+</sup> (10 mM; *A*), Co<sup>2+</sup> (4 mM; *B*), Zn<sup>2+</sup> (1 mM; *C*), or verapamil (1 mM; *D*) in Ca<sup>2+</sup>-Cs<sup>+</sup>-tetraethylammonium external reveals Ca<sup>2+</sup> currents evoked by 10-s square pulses from a -60 mV holding potential (HP) to -50 mV through to -20 mV in 10-mV increments in neurons dialyzed with Cs<sup>+</sup>-Asp-based intracellular solution. Leak currents are eliminated by delivering the voltage steps before and after the block and then subtracting postblock from preblock current. At ≥ -30 mV, steady-state, tonic inward current is evident. *E*: summary graph of mean persistent Ca<sup>2+</sup> current normalized to cell capacitance. Current is calculated as the mean of the last 1 s of the 10-s steps. Ni<sup>2+</sup> reveals significantly more Ca<sup>2+</sup> current relative to the other blockers at -50 mV ( $F_{3,48} = 9.112$ ,  $P < 0.0001$ , 1-way ANOVA;  $P = 0.0007$  Co<sup>2+</sup> vs. Ni<sup>2+</sup>,  $P = 0.0151$  verapamil vs. Ni<sup>2+</sup>,  $P = 0.0002$  Zn<sup>2+</sup> vs. Ni<sup>2+</sup>, Dunnett's multiple comparisons test) and -40 mV ( $H = 16.842$ ,  $df = 3$ ;  $P = 0.0008$ , Kruskal-Wallis 1-way ANOVA;  $P = 0.01495$  Co<sup>2+</sup> vs. Ni<sup>2+</sup>,  $P = 0.0259$  verapamil vs. Ni<sup>2+</sup>,  $P = 0.0012$  Zn<sup>2+</sup> vs. Ni<sup>2+</sup>, Dunn's multiple comparisons test), as well as Zn<sup>2+</sup> and Co<sup>2+</sup> at -30 mV ( $F_{3,48} = 3.633$ ,  $P = 0.0192$ , 1-way ANOVA;  $P = 0.0337$  Co<sup>2+</sup> vs. Ni<sup>2+</sup>,  $P = 0.0927$  verapamil vs. Ni<sup>2+</sup>,  $P = 0.0399$  Zn<sup>2+</sup> vs. Ni<sup>2+</sup>, Dunnett's multiple comparisons test). No significant effects were detected between the blockers at -20 mV ( $F_{3,48} = 2.320$ ,  $P = 0.0871$ , 1-way ANOVA).

## DISCUSSION

The cholinergic receptor responsible for the afterdischarge is ionotropic; the current induced either by pressure ejection or perfusion of acetylcholine is rapid onset and quickly returns to baseline. Yet, the in vitro voltage response to acetylcholine is a prolonged depolarization that greatly outlasts agonist application (10, 26, 28). The afterdischarge itself is supported by Ca<sup>2+</sup>- and/or second messenger-dependent cation channels (12, 19, 54–57). For mammalian neurons, a small number of studies report state switching following ionotropic acetylcholine receptor activation, including burst or persistent firing of hippocampal stratum oriens/alveus interneurons involved in long-term potentiation (LTP) (6), ventral tegmental dopaminergic reward circuitry neurons (7), and hypothalamic hypocretin neurons mediating addiction (58). However, the mechanisms by which these ionotropic receptors cause such change in activity are not well defined. We now show that, for bag cell neurons, the initial depolarization following transient acetylcholine input quickly recruits voltage-dependent persistent Ca<sup>2+</sup> current to drive firing.

Receptor subunit composition could confer distinct mechanisms of action, with variable kinetic, electrophysiological,

and pharmacological properties (59, 60). Our laboratory has found that the bag cell neuron receptor is in part likely comprised of *Aplysia* acetylcholine receptor subunits C and E, which are most similar to mammalian subunits  $\alpha_2$  and  $\alpha_3$ , with 40–50% homology (26). The *Aplysia* current is impermeable to Ca<sup>2+</sup>, has a reversal potential of approximately -15 mV, and is sensitive to the general nicotinic-type inhibitors hexamethonium,  $\alpha$ -conotoxin ImI, and mecamylamine (10, 26). Hexamethonium has previously been found to interact noncompetitively with excitatory ionotropic acetylcholine receptors (61, 62), whereas  $\alpha$ -conotoxin ImI and mecamylamine preferentially inhibit receptors containing  $\alpha_7$  (63) and  $\alpha_3$  (64) subunits, respectively. We used hexamethonium as a positive control to compare the ability of the Ca<sup>2+</sup> channel blockers to inhibit cholinergic current.

Voltage-gated Ca<sup>2+</sup> channels are somewhat distinct from other voltage-gated channels, as they not only contribute to electrical signaling but also couple that signal to changes in intracellular Ca<sup>2+</sup> (65). The effects of voltage-dependent Ca<sup>2+</sup> influx can be “local” by altering the conformation of oxygen-bearing proteins in close proximity to the channel or “global” through Ca<sup>2+</sup>-activated second messengers (65, 66).

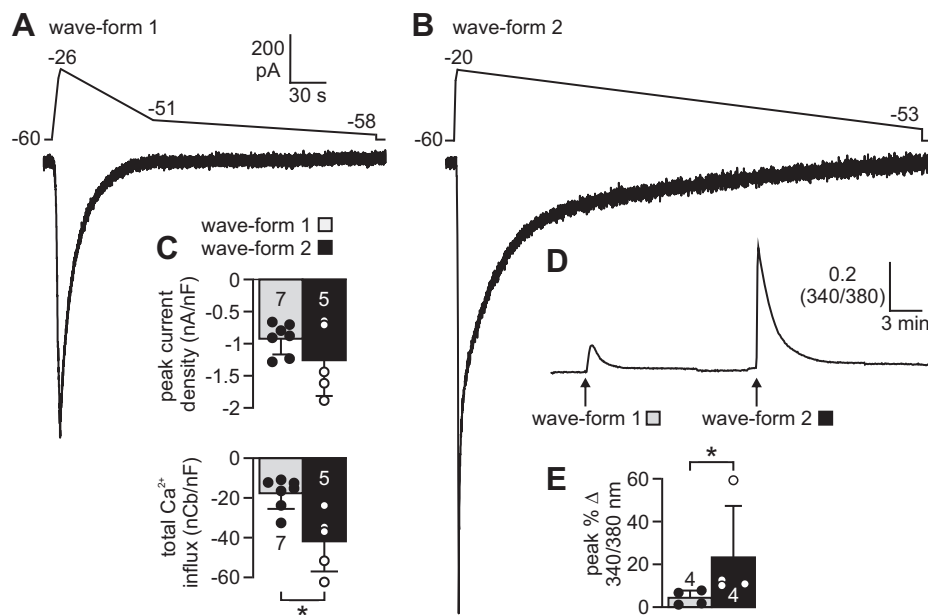


**Figure 7.** Cholinergic-like depolarizing waveforms cause  $\text{Ca}^{2+}$  influx. *A*, top: voltage-ramp waveform mimicking 1 of 2 typical acetylcholine-induced depolarizations (*waveform 1*) is biphasic (see RESULTS text for details). The waveform is applied to a voltage-clamped bag cell neuron bathed in  $\text{Ca}^{2+}$ - $\text{Cs}^+$ -tetraethylammonium artificial seawater (ASW) and dialyzed with  $\text{Cs}^+$ -Asp-based intracellular saline. Leak currents are eliminated by delivering the waveform before and after 4 mM  $\text{Co}^{2+}$  block and then subtracting the postblock current from preblock. *Bottom*: the resulting inward  $\text{Ca}^{2+}$  current. Scale bars apply to both *A* and *B*. *B*, top: voltage-ramp waveform of the second type of acetylcholine-induced depolarization (*waveform 2*), which is essentially monophasic. *Bottom*: the evoked  $\text{Ca}^{2+}$  current is markedly larger compared with that induced by *waveform 1*. *C*: average peak current (top) and  $\text{Ca}^{2+}$  influx (bottom), calculated as area above the curve, both normalized to cell capacitance, during *waveform 1* or *waveform 2*. The peak current density is not significantly different between *waveform 1* and *waveform 2* ( $t_{1,11} = 5.30$ ;  $P = 0.3142$ ; unpaired Student's *t* test, Welch corrected). However, *waveform 2* elicits significantly greater total  $\text{Ca}^{2+}$  influx than *waveform 1* ( $t_{3,13} = 6.05$ ;  $*P = 0.0201$ ; unpaired Student's *t* test). *D*: changes in intracellular  $\text{Ca}^{2+}$  quantified by 340/380 nm ratiometric imaging. Neurons are bathed in normal ASW and dialyzed with  $\text{K}^+$ -Asp-based intracellular saline containing 1 mM fura PE3.  $\text{Ca}^{2+}$  influx is evoked by *waveform 1*, and once the  $\text{Ca}^{2+}$  returns to baseline *waveform 2* is applied, which produces a markedly larger change. *E*: summary of percent change in fluorescence from baseline. *Waveform 2* elicits a significantly greater increase in intracellular  $\text{Ca}^{2+}$  than *waveform 1* ( $U_{4,4} = 9.0$ ;  $*P = 0.0286$ ; Mann-Whitney *U* test). Numbers within the bars are *n* values that reflect number of neurons.

In bag cell neurons, activation of the constitutively expressed voltage-gated  $\text{Ca}^{2+}$  channel Apl  $\text{Ca}_v1$  (32) produces a  $\text{Ca}^{2+}$  current that is fast activating, strongly voltage dependent, slowly inactivating during the pulse, and maximal at approximately +10 mV (12, 17, 27). Apl  $\text{Ca}_v2$ , a covert voltage-gated  $\text{Ca}^{2+}$  channel that is inserted into the membrane by PKC (15, 16, 67, 68), is likely not involved with the initial persistent  $\text{Ca}^{2+}$  conductance, given that PKC activation does not occur for several minutes following afterdischarge onset (69).

Although the acetylcholine-induced current is brief (~1.5 min), the depolarization appears sufficient to sustain the response by gating persistent  $\text{Ca}^{2+}$  current similar to those in other molluscan (30, 70–73) and mammalian (74–76) neurons. The persistent current in bag cell neurons is most likely a “window current” produced within a voltage range where channel activation and inactivation coincide (31). As revealed through leak subtraction with  $\text{Ca}^{2+}$  blockers, the basal Apl  $\text{Ca}_v1$  channel would transition from open to inactivated to closed and then to open again when between –40 and –20 mV (27, 77, 78). This is supported by the ability of the acetylcholine-induced depolarization-like waveforms to evoke  $\text{Ca}^{2+}$  currents or changes to intracellular  $\text{Ca}^{2+}$ . Because the voltage integral appears to be a determinant of  $\text{Ca}^{2+}$  influx, the change in membrane potential during a genuine cholinergic response would itself serve to bolster depolarization.

Generally,  $\text{Ca}^{2+}$  channel blockers either reduce the local  $\text{Ca}^{2+}$  concentration by occupying the constant space charge around the membrane surface or by “charge-screening” (79), as well as competing for binding in the pore (80), and/or binding to regulatory sites on the outside of the channel (81). In bag cell neurons, given that  $\text{Zn}^{2+}$  and verapamil have a lower  $\text{IC}_{50}$  (~300  $\mu\text{M}$ ) and a weaker effect on activation kinetics, they may inhibit by a direct block. Verapamil is presumed to block L-type channels by passing through the membrane in an uncharged state and binding to the inner pore (82, 83), whereas inhibition by  $\text{Zn}^{2+}$  has been attributed to various non-pore-binding sites (35). In squid neurons, although open  $\text{Ca}^{2+}$  channel block by  $\text{Ni}^{2+}$  is voltage independent and thus stabilizes closed states and slows activation kinetics, the inhibition becomes voltage dependent during extended, strong depolarization (84). In barnacle muscle, the amplitude of the current carried by  $\text{Ca}^{2+}$ ,  $\text{Sr}^{2+}$ , or  $\text{Ba}^{2+}$  changes in the presence of  $\text{Co}^{2+}$  (80). Specifically,  $\text{Ba}^{2+}$  currents are greater than  $\text{Ca}^{2+}$  currents under control conditions, likely because of greater affinity of  $\text{Ba}^{2+}$  for the pore. Yet, the block by  $\text{Co}^{2+}$  is far more potent when  $\text{Ba}^{2+}$  is the charge carrier, possibly because of differential competition at the binding site. For bag cell neurons, the presence of  $\text{Co}^{2+}$  within the pore may be responsible for the decidedly right shift in the activation curve.

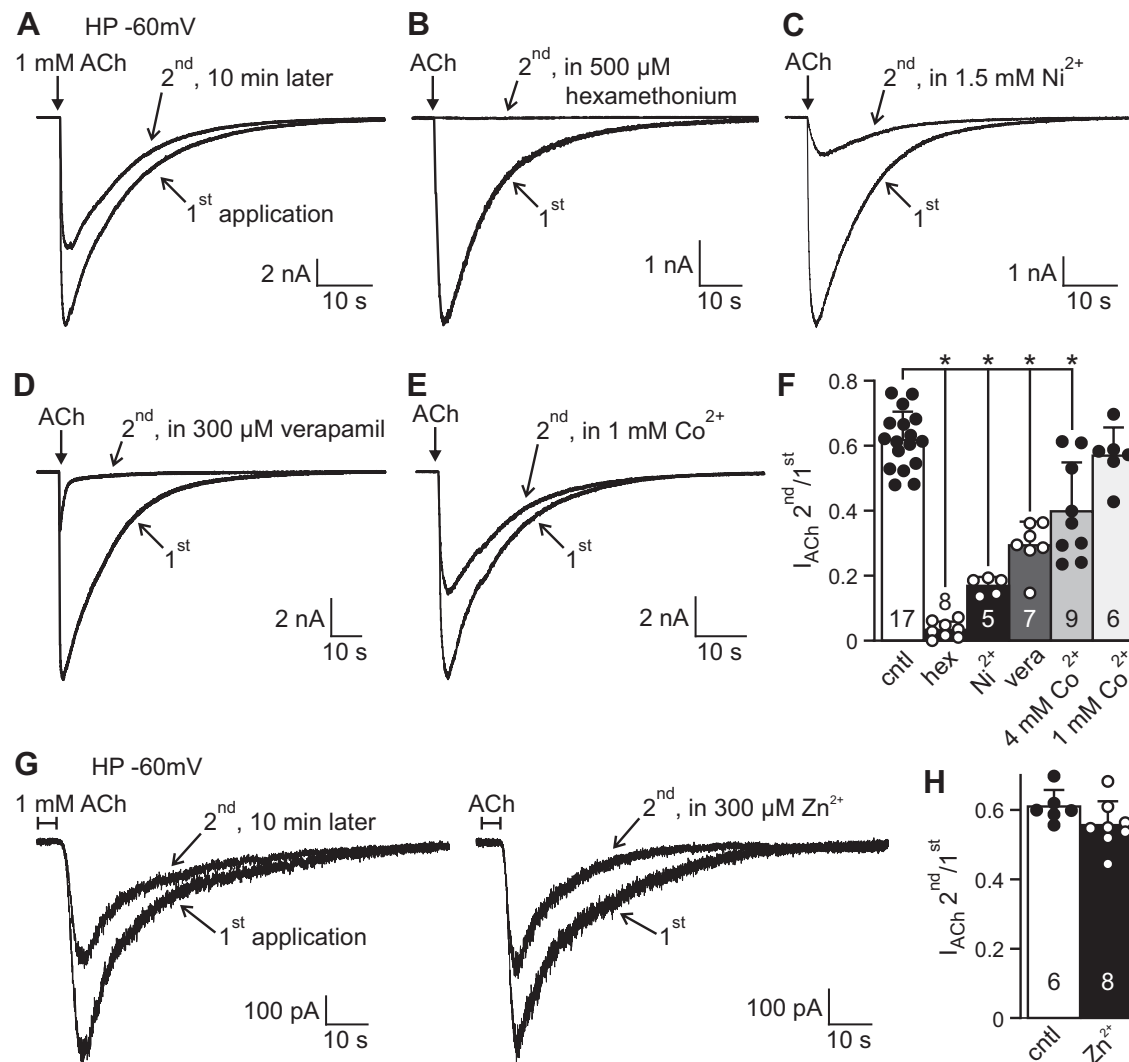


**Figure 8.** The acetylcholine-induced current shows differential sensitivity to hexamethonium,  $Ni^{2+}$ , verapamil,  $Zn^{2+}$ , and  $Co^{2+}$ . **A:** a bag cell neuron is voltage-clamped at  $-60$  mV [holding potential (HP)], bathed in normal artificial seawater, and dialyzed with  $K^+$ -Asp-based intracellular solution. The neuron is pressure-ejected with 1 mM acetylcholine (ACh) for 2 s (at arrow). The resulting current has a rapid onset and lasts  $<1$  min. After a 10-min recovery period, acetylcholine is applied a second time to the same cell; however, the amplitude of the second current is reduced to  $\sim 60\%$  of the first. **B:** extracellular application of the ionotropic acetylcholine receptor blocker hexamethonium ( $500 \mu M$ ), 10 min after the first acetylcholine application, eliminates the second current. **C and D:** delivering the  $IC_{50}$  of the  $Ca^{2+}$  current blockers  $Ni^{2+}$  ( $1.5$  mM; **C**) and verapamil ( $300 \mu M$ ); **D**) also reduces the second acetylcholine-induced current more than control. **E:** delivering the  $IC_{50}$  of  $Co^{2+}$  ( $1.0$  mM) does not suppress the second acetylcholine-induced current compared with control. **F:** average fraction of remaining current ( $I_{ACh}$ ) evoked by the second vs. first acetylcholine application. Compared with control (cntl), there is significantly less residual current in the presence of all blockers except for 1 mM  $Co^{2+}$  ( $F_{6,51} = 2.667$ ,  $P < 0.0001$ , 1-way ANOVA;  $P < 0.0001$  for cntl vs. hex,  $Ni^{2+}$ , verapamil (vera), or 4 mM  $Co^{2+}$ ,  $P = 0.8250$  for cntl vs. 1 mM  $Co^{2+}$ , Dunnett's multiple comparisons test). **G, left:** a 5-s microperfusion of 1 mM acetylcholine (at bar) to the soma of bag cell neuron voltage-clamped at  $-60$  mV evokes a current that desensitizes by  $\sim 60\%$  when acetylcholine is flowed a second time 10 min later. **Right:** superfusion of  $Zn^{2+}$  starting  $\sim 2$  min before the second application of acetylcholine does not alter the extent of desensitization compared with control. **H:** summary data demonstrate no significant difference between fraction of remaining acetylcholine-induced current in the absence or presence of  $Zn^{2+}$  ( $t_{1,71} = 11.97$ ;  $P = 0.1129$ ; unpaired Student's  $t$  test, Welch corrected). Numbers within the bars are  $n$  values that reflect number of neurons.

Vertebrate persistent  $Ca^{2+}$  currents are typically attributed to L-type channels based on defined pharmacological and physiological properties (85, 86). In bag cell neurons,  $\omega$ -conotoxin GVIA, an N-type channel blocker, is largely ineffective; this is not surprising given that the physiological current most closely resembles L-type channels (12, 27). That stated, the Apl  $Ca_v1$  sequence is more similar to dihydropyridine-insensitive, non-L-type vertebrate channels (32), and the current is only partially blocked by large amounts of

dihydropyridine antagonists, such as nifedipine, while being insensitive to dihydropyridine agonists (16, 33). The low sensitivity to nifedipine deterred us from pursuing this blocker in the present study; in addition, nifedipine is reported to inhibit  $K^+$  channels in bag cell channel neurons (33). Given the limited primary structure responsible for dihydropyridine sensitivity (87), the incongruent characteristics of the *Aplysia* channel may be due to select alterations in key residues, thus perhaps rendering a "hybrid-like" channel.

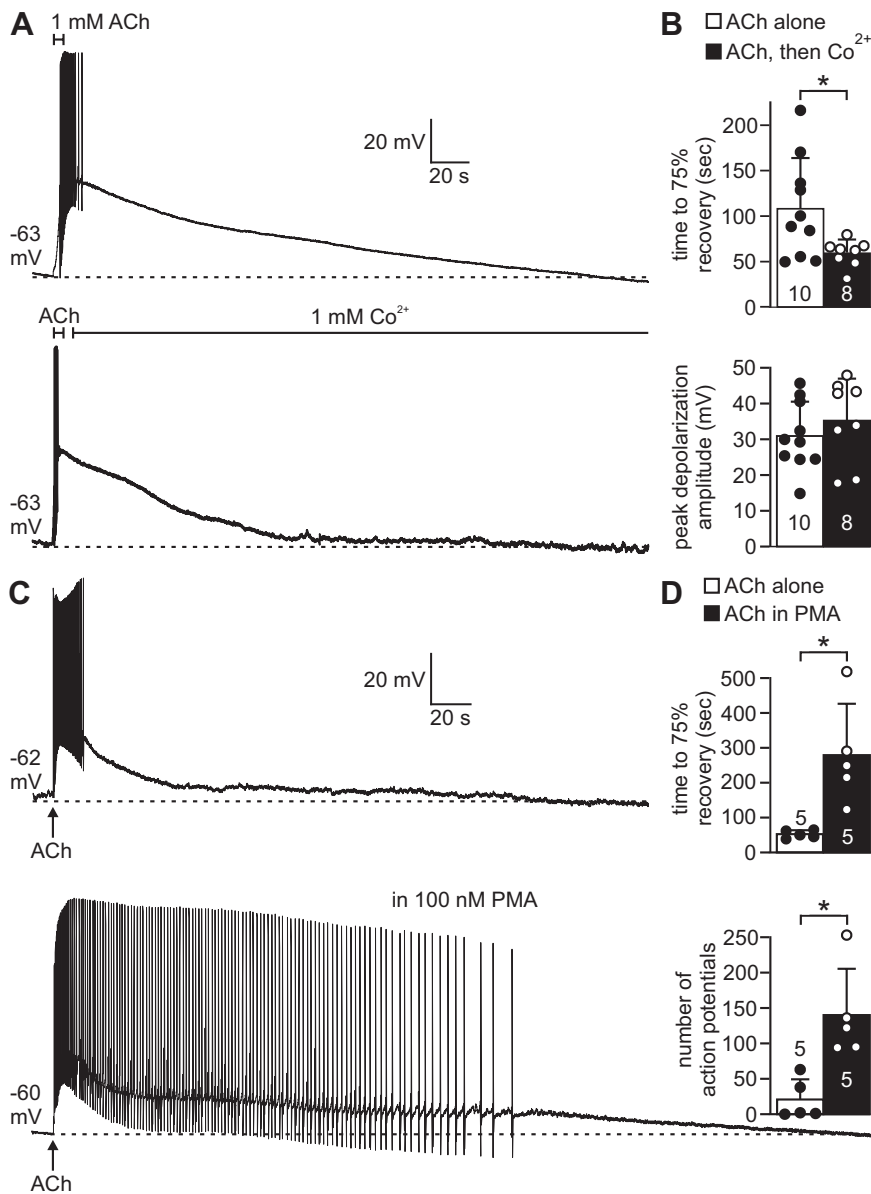


**Figure 9.** The prolonged acetylcholine-induced depolarization is suppressed by  $\text{Co}^{2+}$ . **A**, top: a bag cell neuron is sharp-electrode current-clamped to  $-60$  mV with constant bias current while being perfused with normal artificial seawater (nASW). *Top*: a 5-s perfusion of 1 mM acetylcholine (ACh; at bar) in nASW causes an  $\sim 30$ -mV depolarization with action potentials that lasts  $\sim 2$  min. *Bottom*: in a different neuron, perfusing 1 mM  $\text{Co}^{2+}$   $\sim 5$  s after acetylcholine causes the depolarization to subside more rapidly. **B**, top: summary data show that the time to 75% recovery in neurons exposed to acetylcholine alone is significantly different from  $\text{Co}^{2+}$  after acetylcholine ( $t_{2,70} = 10.53$ ;  $*P = 0.0214$ ; unpaired Student's  $t$  test). *Bottom*: average peak depolarization amplitude is not significantly different between neurons superfused with acetylcholine and those receiving  $\text{Co}^{2+}$  after acetylcholine ( $t_{0,84} = 13.45$ ;  $P = 0.4178$ ; unpaired Student's  $t$  test). **C**, top: a 2-s pressure ejection of acetylcholine in nASW results in an  $\sim 27$ -mV depolarization with  $\sim 20$  spikes lasting  $\sim 1$  min. *Bottom*: in a different neuron pretreated with 100 nM phorbol 12-myristate 13-acetate (PMA) for  $\sim 20$  min, acetylcholine evokes an  $\sim 38$ -mV depolarization with  $\sim 140$  spikes lasting  $\sim 5$  min. **D**, top: group data establish that time to 75% recovery in control neurons returns to baseline significantly faster than in PMA-pretreated neurons ( $t_{3,43} = 4.05$ ;  $*P = 0.026$ ; unpaired Student's  $t$  test). *Bottom*: mean number of action potentials in neurons with PMA is higher than that of control during acetylcholine-induced depolarization ( $t_{3,72} = 5.46$ ;  $*P = 0.0117$ ; unpaired Student's  $t$  test). Numbers within the bars are  $n$  values that reflect number of neurons.

Even though  $\text{Co}^{2+}$ ,  $\text{Ni}^{2+}$ ,  $\text{Zn}^{2+}$ , and verapamil are widely used as  $\text{Ca}^{2+}$  channel blockers, they are not completely selective; here, the  $\text{IC}_{100}$  of the blockers also suppressed acetylcholine-induced currents.  $\text{Co}^{2+}$  is reported to inhibit cholinergic as well as  $\text{GABA}_A$  and glutamatergic receptors in hippocampal pyramidal cells (88).  $\text{Ni}^{2+}$  reduces the acetylcholine-induced current at the frog neuromuscular junction by decreasing single-channel conductance (89). Verapamil decreases the opening frequency of cholinergic receptors in mouse neuromuscular junction, accelerating channel desensitization (90). Interestingly,  $\text{Zn}^{2+}$  can potentiate ionotropic acetylcholine receptors expressed in *Xenopus* oocytes by increasing burst duration and channel open probability depending on the subunit ( $\alpha_{2-4}$ ,  $\beta_{2,4}$ ) (91–93). In chicken  $\alpha_7$  neuronal ionotropic acetylcholine receptors, again expressed in oocytes,  $\text{Zn}^{2+}$  exhibits a competitive and voltage-independent block (94). Our investigation of bag cell neurons ultimately found that an  $\text{IC}_{50}$  concentration of  $\text{Co}^{2+}$  does

not affect the cholinergic current, making it a suitable pharmacological tool.

The persistent voltage-dependent  $\text{Ca}^{2+}$  current appears to be recruited by the acetylcholine-induced depolarization; when persistent  $\text{Ca}^{2+}$  current is inhibited with  $\text{Co}^{2+}$  shortly after depolarization onset the duration is attenuated, and when the  $\text{Ca}^{2+}$  current is promoted by PKC activation the response is prolonged. We did not observe a truncation of the depolarization or bursting with  $\text{Co}^{2+}$ , most likely because we used the  $\text{IC}_{50}$ . Moreover, PMA does not alter the acetylcholine-induced current (28), and thus PKC probably enhances the acetylcholine-induced depolarization, in part, by supporting the persistent  $\text{Ca}^{2+}$  current (27). This is highlighted by the approximately sevenfold increase in action potential firing in the presence of acetylcholine and PMA compared with acetylcholine alone.

Our previous work found that voltage-gated  $\text{Ca}^{2+}$  entry during a 5-Hz, 10-s train of action potentials triggers a

voltage-independent cation current and prolonged depolarization (12). However, it is unknown whether  $\text{Ca}^{2+}$  influx during the initial acetylcholine-induced depolarization recruits such cation channels, which in turn may engage persistent  $\text{Ca}^{2+}$  current or extend the response on their own. Regardless,  $\text{Apl Ca}_v1$  is probably first opened by the cholinergic depolarization, which might serve to reach a threshold concentration of intracellular  $\text{Ca}^{2+}$  and/or bring about a pattern of free  $\text{Ca}^{2+}$  required for a bona fide afterdischarge. Overall, voltage-dependent  $\text{Ca}^{2+}$  influx appears to be a key factor in the control of bag cell neuron responsiveness and potentially afterdischarge initiation. The change in firing following ionotropic receptor activation is very similar to that seen in other systems following metabotropic receptor activation, suggesting that distinct cholinergic pathways may achieve similar ends at the level of neuronal output.

## DATA AVAILABILITY

Original data sets are available from the corresponding author on reasonable request.

## GRANTS

This work was supported by a Canadian Institutes of Health Research project grant (PJT-159794) to N.S.M.

## DISCLOSURES

No conflicts of interest, financial or otherwise, are declared by the authors.

## AUTHOR CONTRIBUTIONS

K.H.L. and N.S.M. conceived and designed research; K.H.L., D.E.W., and E.K.M. performed experiments; K.H.L., D.E.W., and E.K.M. analyzed data; K.H.L. and N.S.M. interpreted results of experiments; K.H.L. prepared figures; K.H.L. drafted manuscript; K.H.L. and N.S.M. edited and revised manuscript; K.H.L. and N.S.M. approved final version of manuscript.

## REFERENCES

- Haj-Dahmane S, Andrade R. Muscarinic activation of a voltage-dependent cation nonselective current in rat association cortex. *J Neurosci* 16: 3848–3861, 1996. doi:10.1523/JNEUROSCI.16-12-03848.1996.
- Egorov AV, Hamam BN, Fransén E, Hasselmo ME, Alonso AA. Graded persistent activity in entorhinal cortex neurons. *Nature* 420: 173–178, 2002. doi:10.1038/nature01171.
- Zhang Z, Reboreda A, Alonso A, Barker PA, Séguéla P. TRPC channels underlie cholinergic plateau potentials and persistent activity in entorhinal cortex. *Hippocampus* 21: 386–397, 2011. doi:10.1002/hipo.20755.
- Baker AL, O'Toole RJ, Gullledge AT. Preferential cholinergic excitation of corticopontine neurons. *J Physiol* 596: 1659–1679, 2018. doi:10.1113/JP275194.
- Fu X, Ye H, Jia H, Wang X, Chomiak T, Luo F. Muscarinic acetylcholine receptor-dependent persistent activity of layer 5 intrinsic-bursting and regular-spiking neurons in primary auditory cortex. *J Neurophysiol* 122: 2344–2353, 2019. doi:10.1152/jn.00184.2019.
- Jia Y, Yamazaki Y, Nakauchi S, Sumikawa K.  $\alpha 2$  Nicotinic receptors function as a molecular switch to continuously excite a subset of interneurons in rat hippocampal circuits. *Eur J Neurosci* 29: 1588–1603, 2009. doi:10.1111/j.1460-9568.2009.06706.x.
- Liu L, Zhao-Shea R, McIntosh JM, Gardner PD, Tapper AR. Nicotine persistently activates ventral tegmental area dopaminergic neurons via nicotinic acetylcholine receptors containing  $\alpha 4$  and  $\alpha 6$  subunits. *Mol Pharmacol* 81: 541–548, 2012. doi:10.1124/mol.111.076661.
- Kupfermann I, Kandel ER. Electrophysiological properties and functional interconnections of two symmetrical neurosecretory clusters (bag cells) in abdominal ganglion of *Aplysia*. *J Neurophysiol* 33: 865–876, 1970. doi:10.1152/jn.1970.33.6.865.
- Kaczmarek LK, Jennings KR, Strumwasser F. An early sodium and a late calcium phase in the afterdischarge of peptide-secreting neurons of *Aplysia*. *Brain Res* 238: 105–115, 1982. doi:10.1016/0006-8993(82)90774-0.
- White SH, Magoski NS. Acetylcholine-evoked afterdischarge in *Aplysia* bag cell neurons. *J Neurophysiol* 107: 2672–2685, 2012. doi:10.1152/jn.00745.2011.
- Fisher TE, Levy S, Kaczmarek LK. Transient changes in intracellular calcium associated with a prolonged increase in excitability in neurons of *Aplysia californica*. *J Neurophysiol* 71: 1254–1257, 1994. doi:10.1152/jn.1994.71.3.1254.
- Hung AY, Magoski NS. Activity-dependent initiation of a prolonged depolarization in *Aplysia* bag cell neurons: role for a cation channel. *J Neurophysiol* 97: 2465–2479, 2007. doi:10.1152/jn.00941.2006.
- Geiger JE, Magoski NS.  $\text{Ca}^{2+}$ -induced  $\text{Ca}^{2+}$  release in *Aplysia* bag cell neurons requires interaction between mitochondrial and endoplasmic reticulum stores. *J Neurophysiol* 100: 24–37, 2008. doi:10.1152/jn.90356.2008.
- Groten CJ, Rebane JT, Blohm G, Magoski NS. Separate  $\text{Ca}^{2+}$  sources are buffered by distinct  $\text{Ca}^{2+}$  handling systems in *Aplysia* neuroendocrine cells. *J Neurosci* 33: 6476–6491, 2013. doi:10.1523/JNEUROSCI.6384-11.2013.
- DeRiemer SA, Strong JA, Albert KA, Greengard P, Kaczmarek LK. Enhancement of calcium current in *Aplysia* neurons by phorbol ester and protein kinase C. *Nature* 313: 313–316, 1985. doi:10.1038/313313a0.
- Strong JA, Fox AP, Tsien RW, Kaczmarek LK. Stimulation of protein kinase C recruits covert calcium channels in *Aplysia* bag cell neurons. *Nature* 325: 714–717, 1987. doi:10.1038/325714a0.
- Groten CJ, Magoski NS. PKC enhances the capacity for secretion by rapidly recruiting covert voltage-gated  $\text{Ca}^{2+}$  channels to the membrane. *J Neurosci* 35: 2747–2765, 2015. doi:10.1523/JNEUROSCI.3581-14.2015.
- Hickey CM, Geiger JE, Groten CJ, Magoski NS. Mitochondrial  $\text{Ca}^{2+}$  activates a cation current in *Aplysia* bag cell neurons. *J Neurophysiol* 103: 1543–1556, 2010 [Erratum in *J Neurophysiol* 103: 2934, 2010]. doi:10.1152/jn.01121.2009.
- Sturgeon RM, Magoski NS. Diacylglycerol-mediated regulation of *Aplysia* bag cell neuron excitability requires protein kinase C. *J Physiol* 594: 5573–5592, 2016. doi:10.1113/JP272152.
- Wilson GF, Richardson FC, Fisher TE, Olivera BM, Kaczmarek LK. Identification and characterization of a  $\text{Ca}^{2+}$ -sensitive nonspecific cation channel underlying prolonged repetitive firing in *Aplysia* neurons. *J Neurosci* 16: 3661–3671, 1996. doi:10.1523/JNEUROSCI.16-11-03661.1996.
- Lupinsky DA, Magoski NS.  $\text{Ca}^{2+}$ -dependent regulation of non-selective cation channel from *Aplysia* bag cell neurons. *J Physiol* 575: 491–506, 2006. doi:10.1113/jphysiol.2006.105833.
- Chauhan AK, Magoski NS. Hydrogen peroxide gates a voltage-dependent cation current in *Aplysia* neuroendocrine cells. *J Neurosci* 39: 9900–9913, 2019. doi:10.1523/JNEUROSCI.1460-19.2019.
- Pinsker HM, Dudek FE. Bag cell control of egg laying in freely behaving *Aplysia*. *Science* 197: 490–493, 1977. doi:10.1126/science.197.4302.490.
- Stuart DK, Strumwasser F. Neuronal sites of action of a neurosecretory peptide, egg-laying hormone, in *Aplysia californica*. *J Neurophysiol* 43: 499–519, 1980. doi:10.1152/jn.1980.43.2.499.
- Loechner KJ, Azhderian EM, Dreyer R, Kaczmarek LK. Progressive potentiation of peptide release during a neuronal discharge. *J Neurophysiol* 63: 738–744, 1990. doi:10.1152/jn.1990.63.4.738.
- White SH, Carter CJ, Magoski NS. A potentially novel nicotinic receptor in *Aplysia* neuroendocrine cells. *J Neurophysiol* 112: 446–462, 2014. doi:10.1152/jn.00796.2013.
- Tam AK, Geiger JE, Hung AY, Groten CJ, Magoski NS. Persistent  $\text{Ca}^{2+}$  current contribute to a prolonged depolarization in *Aplysia* bag cell neurons. *J Neurophysiol* 102: 3753–3765, 2009. doi:10.1152/jn.00669.2009.
- White SH, Sturgeon RM, Gu Y, Nensi A, Magoski NS. Tyrosine phosphorylation determines afterdischarge initiation by ionotropic cholinergic receptor. *Neuroscience* 372: 273–288, 2018. doi:10.1016/j.neuroscience.2017.12.049.

29. Grynkiwicz G, Poenie M, Tsien RY. A new generation of  $\text{Ca}^{2+}$  indicators with greatly improved fluorescence properties. *J Biol Chem* 260: 3440–3450, 1985. doi:10.1016/S0021-9258(19)83641-4.
30. Eckert R, Lux HD. A voltage-sensitive persistent calcium conductance in neuronal soma of *Helix*. *J Physiol* 254: 129–151, 1976. doi:10.1113/jphysiol.1976.sp011225.
31. Attwell D, Cohen I, Eisner D, Ohba M, Ojeda C. The steady state TTX-sensitive (“window”) sodium current in cardiac Purkinje fibres. *Pflügers Arch* 379: 137–142, 1979. doi:10.1007/BF00586939.
32. White BH, Kaczmarek LK. Identification of a vesicular pool of calcium channels in the bag cell neurons of *Aplysia californica*. *J Neurosci* 17: 1582–1595, 1997. doi:10.1523/JNEUROSCI.17-05-01582.1997.
33. Nerbonne JM, Gurney AM. Blockade of  $\text{Ca}^{2+}$  and  $\text{K}^{+}$  currents in bag cell neurons of *Aplysia californica* by dihydropyridine  $\text{Ca}^{2+}$  antagonists. *J Neurosci* 7: 882–893, 1987. doi:10.1523/JNEUROSCI.07-03-00882.1987.
34. Pellmar TC. Enhancement of inward current by serotonin in neurons of *Aplysia*. *J Neurobiol* 15: 13–25, 1984. doi:10.1002/neu.480150103.
35. Büsselberg D, Evans ML, Rahmann H, Carpenter DO.  $\text{Zn}^{2+}$  blocks the voltage activated calcium current of *Aplysia* neurons. *Neurosci Lett* 117: 117–122, 1990. doi:10.1016/0304-3940(90)90129-W.
36. Tamse CT, Hammar K, Porterfield DM, Smith PJ. Transmembrane calcium flux in  $\text{Pb}^{2+}$ -exposed *Aplysia* neurons. *Biol Bull* 195: 201–202, 1998. doi:10.2307/1542838.
37. Henquin JC, Lambert AE. Cobalt inhibition of insulin secretion and calcium uptake by isolated rat islets. *Am J Physiol* 228: 1669–1677, 1975. doi:10.1152/ajplegacy.1975.228.6.1669.
38. Moger WH. Effects of the calcium-channel blockers cobalt, verapamil, and D600 on Leydig cell steroidogenesis. *Biol Reprod* 28: 528–535, 1983. doi:10.1095/biolreprod28.3.528.
39. Büsselberg D, Michael D, Evans ML, Carpenter DO, Haas HL. Zinc ( $\text{Zn}^{2+}$ ) blocks voltage gated calcium channels in cultured rat dorsal root ganglion cells. *Brain Res* 593: 77–81, 1992. doi:10.1016/0006-8993(92)91266-H.
40. Hagiwara S, Byerly L. Calcium channel. *Annu Rev Neurosci* 4: 69–125, 1981. doi:10.1146/annurev.ne.04.030181.000441.
41. Swandulla D, Armstrong CM. Calcium channel block by cadmium in chicken sensory neurons. *Proc Natl Acad Sci USA* 86: 1736–1740, 1989. doi:10.1073/pnas.86.5.1736.
42. Chow RH. Cadmium block of squid calcium currents: macroscopic data and kinetic model. *J Gen Physiol* 98: 751–770, 1991. doi:10.1085/jgp.98.4.751.
43. Shen JB, Jiang B, Pappano AJ. Comparison of L-type calcium channel blockade by nifedipine and/or cadmium in guinea pig ventricular myocytes. *J Pharmacol Exp Ther* 294: 562–570, 2000.
44. Cruz LJ, Johnson DS, Olivera BM. Characterization of the omega conotoxin target. Evidence for tissue specific heterogeneity in calcium channel types. *Biochemistry* 26: 820–824, 1987. doi:10.1021/bi00377a024.
45. Pruneau D, Angus JA. Omega-conotoxin GVIA is a potent inhibitor of sympathetic neurogenic responses in rat small mesenteric arteries. *Br J Pharmacol* 100: 180–184, 1990. doi:10.1111/j.1476-5381.1990.tb12073.x.
46. Robitaille R, Adler EM, Charlton MP. Strategic location of calcium channels at transmitter release sites of frog neuromuscular synapses. *Neuron* 5: 773–779, 1990. doi:10.1016/0896-6273(90)90336-E.
47. Sato K, Park NG, Kohno T, Maeda T, Kim JI, Kato R, Takahashi M. Role of basic residues for the binding of  $\omega$ -conotoxin GIVA to N-type calcium channels. *Biochem Biophys Res Commun* 194: 1292–1296, 1993. doi:10.1006/bbrc.1993.1964.
48. Connor JA, Kretz R, Shapiro E. Calcium levels measured in a presynaptic neurone of *Aplysia* under conditions that modulate transmitter release. *J Physiol* 375: 625–642, 1986. doi:10.1113/jphysiol.1986.sp016137.
49. Edmonds B, Klein M, Dale N, Kandel ER. Contributions of two types of calcium channels to synaptic transmission and plasticity. *Science* 250: 1142–1147, 1990. doi:10.1126/science.2174573.
50. Trudeau LE, Baux G, Fossier P, Tauc L. Transmitter release and calcium currents at an *Aplysia* buccal ganglion synapse—I. Characterization. *J Neurosci* 53: 571–580, 1993. doi:10.1016/0306-4522(93)90222-2.
51. Fossier P, Baux G, Tauc L. N- and P-type  $\text{Ca}^{2+}$  channels are involved in acetylcholine release at a neuron-neuron synapse: only the N-type channel is the target of neuromodulators. *Proc Natl Acad Sci USA* 91: 4771–4775, 1994. doi:10.1073/pnas.91.11.4771.
52. Noh S, Lee SR, Jeong YJ, Ko KS, Rhee BD, Kim N, Han J. The direct modulatory activity of zinc toward ion channels. *Integr Med Res* 4: 142–146, 2015. doi:10.1016/j.imr.2015.07.004.
53. Castagna M, Takai Y, Kaibuchi K, Sano K, Kikkawa U, Nishizuka Y. Direct activation of calcium-activated, phospholipid-dependent protein kinase by tumor-promoting phorbol esters. *J Biol Chem* 257: 7847–7851, 1982. doi:10.1016/S0021-9258(18)34459-4.
54. Magoski NS, Wilson GF, Kaczmarek LK. Protein kinase modulation of a neuronal cation channel requires protein-protein interactions mediated by an Src homology 3 domain. *J Neurosci* 22: 1–9, 2002. doi:10.1523/JNEUROSCI.22-01-00001.2002.
55. Magoski NS. Regulation of an *Aplysia* bag cell neuron cation channel by closely associated protein kinase A and a protein phosphatase. *J Neurosci* 24: 6833–6841, 2004. doi:10.1523/JNEUROSCI.1694-04.2004.
56. Magoski NS, Kaczmarek LK. Association/dissociation of a channel-kinase complex underlies state-dependent modulation. *J Neurosci* 25: 8037–8047, 2005 [Erratum in *J Neurosci* 25:8588, 2005]. doi:10.1523/JNEUROSCI.1903-05.2005.
57. Sturgeon RM, Magoski NS. A closely associated phospholipase C regulates cation channel function through phosphoinositide hydrolysis. *J Neurosci* 38: 7622–7634, 2018. doi:10.1523/JNEUROSCI.0586-18.2018.
58. Zhou WL, Gao XB, Picciotto MR. Acetylcholine acts through nicotinic receptors to enhance the firing rate of a subset of hypocretin neurons in the mouse hypothalamus through distinct presynaptic and postsynaptic mechanisms. *eNeuro* 2: ENEURO.0052-14.2015, 2015. doi:10.1523/ENEURO.0052-14.2015.
59. Nelson ME, Lindstrom J. Single channel properties of human  $\alpha 3$  AChRs: impact of  $\beta 2$ ,  $\beta 4$  and  $\alpha 5$  subunits. *J Physiol* 516: 657–678, 1999. doi:10.1111/j.1469-7793.1999.0657u.x.
60. Wang H, Sun X. Desensitized nicotinic receptors in brain. *Brain Res Brain Res Rev* 48: 420–437, 2005. doi:10.1016/j.brainresrev.2004.09.003.
61. Tauc L, Gerschenfeld HM. A cholinergic mechanism of inhibitory synaptic transmission in a molluscan nervous system. *J Neurophysiol* 25: 236–262, 1962. doi:10.1152/jn.1962.25.2.236.
62. Kehoe J. Three acetylcholine receptors in *Aplysia* neurons. *J Physiol* 225: 115–146, 1972. doi:10.1113/jphysiol.1972.sp009931.
63. Johnson DS, Martinez J, Elgoyhen AB, Heinemann SF, McIntosh JM. Alpha-conotoxin Iml exhibits subtype-specific nicotinic acetylcholine receptor blockade: preferential inhibition of homomeric  $\alpha 7$  and  $\alpha 9$  receptors. *Mol Pharmacol* 48: 194–199, 1995.
64. Papke R, Sanberg P, Shytle R. Analysis of mecamylamine stereoisomers on human nicotinic receptor subtypes. *J Pharmacol Exp Ther* 287: 646–656, 2001.
65. Clapham DE. Calcium signalling. *Cell* 131: 1047–1058, 2007. doi:10.1016/j.cell.2007.11.028.
66. Ikeda SR. Calcium channels—link locally, act globally. *Science* 294: 318–319, 2001. doi:10.1126/science.1066160.
67. Conn PJ, Strong JA, Kaczmarek LK. Inhibitors of protein kinase C prevent enhancement of calcium current and action potentials in peptidergic neurons of *Aplysia*. *J Neurosci* 9: 480–487, 1989. doi:10.1523/JNEUROSCI.09-02-00480.1989.
68. Zhang Y, Helm JS, Senatore A, Spafford JD, Kaczmarek LK, Jonas EA. PKC-induced intracellular trafficking of  $\text{Ca}_v2$  precedes its rapid recruitment to the plasma membrane. *J Neurosci* 28: 2601–2612, 2008. doi:10.1523/JNEUROSCI.4314-07.
69. Wayne NL, Lee W, Kim YJ. Persistent activation of calcium-activated and calcium-independent protein kinase C in response to electrical afterdischarge from peptidergic neurons of *Aplysia*. *Brain Res* 834: 211–213, 1999. doi:10.1016/S0006-8993(99)01594-2.
70. Adams DJ, Gage PW. Characteristics of sodium and calcium conductance changes produced by membrane depolarization in an *Aplysia* neurone. *J Physiol* 289: 143–161, 1979. doi:10.1113/jphysiol.1979.sp012729.
71. Plant TD, Standen NB. Calcium current inactivation in identified neurones of *Helix aspersa*. *J Physiol* 321: 273–285, 1981. doi:10.1113/jphysiol.1981.sp013983.
72. Chad J, Eckert R, Ewald D. Kinetics of calcium-dependent inactivation of calcium current in voltage-clamped neurones of *Aplysia californica*. *J Physiol* 347: 279–300, 1984. doi:10.1113/jphysiol.1984.sp015066.

73. **Oyama Y, Akaike N, Nishi K.** Persistent calcium inward current in internally perfused snail neuron. *Cell Mol Neurobiol* 6: 71–85, 1986. doi:10.1007/BF00742977.
74. **Beam KG, Knudson CM.** Effect of postnatal development on calcium currents and slow charge movement in mammalian skeletal muscle. *J Gen Physiol* 91: 799–815, 1988. doi:10.1085/jgp.91.6.799.
75. **Hounsgaard J, Kiehn O.** Serotonin-induced bistability of turtle motoneurons caused by a nifedipine-sensitive calcium plateau potential. *J Physiol* 414: 265–282, 1989. doi:10.1113/jphysiol.1989.sp017687.
76. **Booth V, Rinzel J, Kiehn O.** Compartmental model of vertebrate motoneurons for  $\text{Ca}^{2+}$ -dependent spiking and plateau potentials under pharmacological treatment. *J Neurophysiol* 78: 3371–3385, 1997. doi:10.1152/jn.1997.78.6.3371.
77. **Cohen NM, Lederer WJ.** Calcium current in isolated neonatal rat ventricular myocytes. *J Physiol* 391: 169–191, 1987. doi:10.1113/jphysiol.1987.sp016732.
78. **Reuter H, Scholz H.** The regulation of the calcium conductance of cardiac muscle by adrenaline. *J Physiol* 264: 49–62, 1977. doi:10.1113/jphysiol.1977.sp011657.
79. **Muller RU, Finkelstein A.** The electrostatic basis of  $\text{Mg}^{2+}$  inhibition of transmitter release. *Proc Natl Acad Sci USA* 71: 923–926, 1974. doi:10.1073/pnas.71.3.923.
80. **Hagiwara S, Fukuda J, Eaton DC.** Membrane currents carried by  $\text{Ca}^{2+}$ ,  $\text{Sr}^{2+}$  and  $\text{Ba}^{2+}$  in barnacle muscle fibre during voltage clamp. *J Gen Physiol* 63: 564–578, 1974. doi:10.1085/jgp.63.5.564.
81. **Kostyuk PG, Mironov SL, Shuba YM.** Two ion-selecting filters in the calcium channel of the somatic membrane of mollusc neurons. *J Membr Biol* 76: 83–93, 1983. doi:10.1007/BF01871455.
82. **Hescheler J, Pelzer D, Trube G, Trautwein W.** Does organic calcium channel blocker D600 act from inside or outside on the cardiac cell membrane? *Pflugers Arch* 393: 287–291, 1982. doi:10.1007/BF00581411.
83. **Hockerman GH, Peterson BZ, Johnson BD, Catterall WA.** Molecular determinants of drug binding on L-type calcium channels. *Annu Rev Pharmacol Toxicol* 37: 361–396, 1997. doi:10.1146/annurev.pharmtox.37.1.361.
84. **McFarlane MB, Gilly WF.** State-dependent nickel block of a high-voltage-activated neuronal calcium channel. *J Neurophysiol* 80: 1678–1685, 1998. doi:10.1152/jn.1998.80.4.1678.
85. **Carlin KP, Jones KE, Jiang Z, Jordan LM, Brownstone RM.** Dendritic L-type calcium currents in mouse spinal motoneurons: implications for bistability. *Eur J Neurosci* 12: 1635–1646, 2000. doi:10.1046/j.1460-9568.2000.00055.x.
86. **Moritz AT, Newkirk G, Powers RK, Binder MD.** Facilitation of somatic calcium channels can evoke prolonged tail currents in rat hypoglossal motoneurons. *J Neurophysiol* 98: 1042–1047, 2007. doi:10.1152/jn.01294.2006.
87. **Grabner M, Wang Z, Hering S, Striessnig J, Glossmann H.** Transfer of 1,4-dihydropyridine sensitivity from L-type to class A (BI) calcium channels. *Neuron* 16: 207–218, 1996. doi:10.1016/S0896-6273(00)80037-9.
88. **Gerber U, Gähwiler BH.** Cobalt blocks postsynaptic responses induced by neurotransmitters in the hippocampus in vitro. *Neurosci Lett* 134: 53–56, 1991. doi:10.1016/0304-3940(91)90507-P.
89. **Magleby KL, Weinstock MM.** Nickel and calcium ions modify the characteristics of the acetylcholine receptor-channel complex at the frog neuromuscular junction. *J Physiol* 299: 203–218, 1980. doi:10.1113/jphysiol.1980.sp013120.
90. **Wachtel RE.** Effects of diltiazem and verapamil on responses to acetylcholine. *Br J Pharmacol* 92: 561–566, 1987. doi:10.1111/j.1476-5381.1987.tb11357.x.
91. **Hsiao B, Dweck D, Luetje CW.** Subunit-dependent modulation of neuronal nicotinic receptors by zinc. *J Neurosci* 21: 1848–1856, 2001. doi:10.1523/JNEUROSCI.21-06-01848.2001.
92. **Hsiao B, Mihalak KB, Repicky SE, Everhart D, Mederos AH, Malhotra A, Luetje CW.** Determinants of zinc potentiation on the 4 subunit of neuronal nicotinic receptors. *Mol Pharmacol* 69: 27–36, 2006. doi:10.1124/mol.105.015164.
93. **Hsiao B, Mihalak KB, Magleby KL, Luetje CW.** Zinc potentiates neuronal nicotinic receptors by increasing burst duration. *J Neurophysiol* 99: 999–1007, 2008. doi:10.1152/jn.01040.2007.
94. **Palma E, Maggi L, Miledi R, Eusebi F.** Effects of  $\text{Zn}^{2+}$  on wild and mutant neuronal  $\alpha 7$  nicotinic receptors. *Proc Natl Acad Sci USA* 95: 10246–10250, 1998. doi:10.1073/pnas.95.17.10246.